ESPOO 2003 VTT PUBLICATIONS 502

Mika Bäckström

Multiaxial fatigue life assessment of welds based on nominal and hot spot stresses

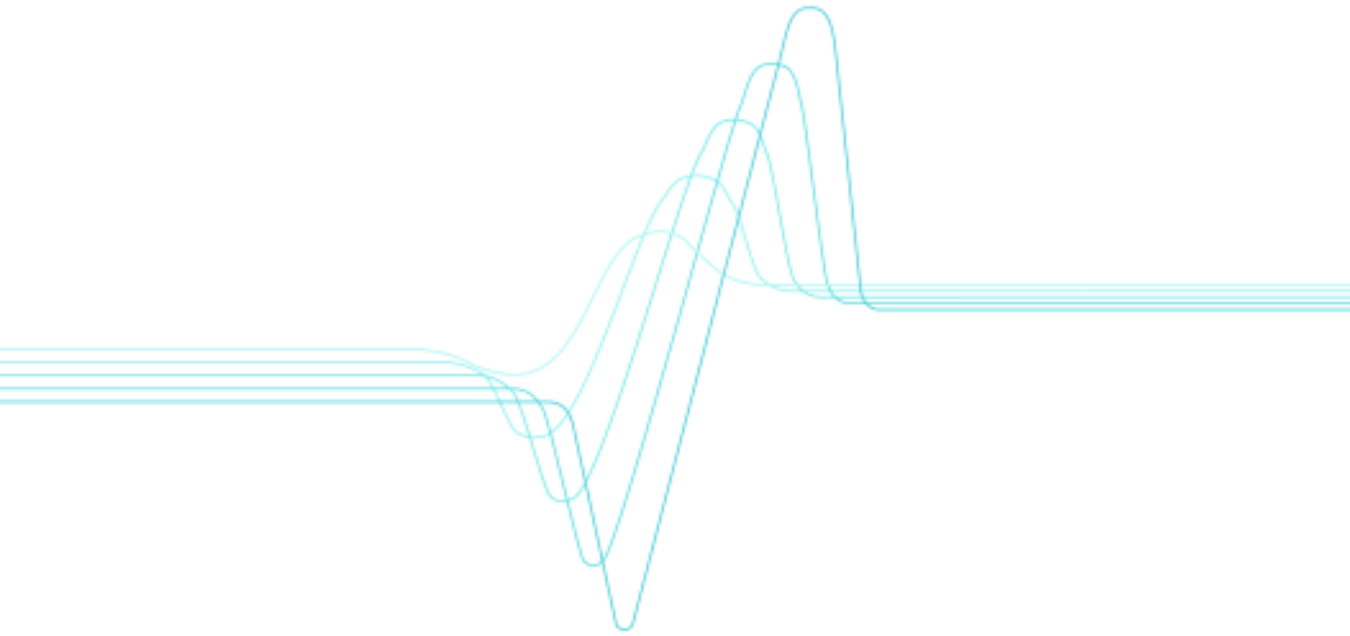

VTT PUBLICATIONS 502

Multiaxial fatigue life assessment of welds based on nominal and hot spot stresses

Mika Bäckström

VTT Industrial Systems

Thesis for the degree of Doctor of Science in Technology to be presented with due permission for public examination and criticism in the Auditorium 1383 at Lappeenranta University of Technology (Lappeenranta, Finland) on the 13th of August, 2003, at 12 o'clock noon.

ISBN 951–38–6233–X (soft back ed.)
ISSN 1235–0621 (soft back ed.)

ISBN 951–38–6234–8 (URL: http://www.vtt.fi/inf/pdf/)
ISSN 1455–0849 (URL: http://www.vtt.fi/inf/pdf/)

JULKAISIJA – UTGIVARE – PUBLISHER

VTT, Vuorimiehentie 5, PL 2000, 02044 VTT
puh. vaihde (09) 4561, faksi (09) 456 4374

VTT, Bergsmansvägen 5, PB 2000, 02044 VTT
tel. växel (09) 4561, fax (09) 456 4374

VTT Technical Research Centre of Finland, Vuorimiehentie 5, P.O.Box 2000, FIN–02044 VTT, Finland
phone internat. + 358 9 4561, fax + 358 9 456 4374

VTT Tuotteet ja tuotanto, Otakaari 7 B, PL 1705, 02044 VTT
puh. vaihde (09) 4561, faksi (09) 456 7039

VTT Industriella System, Otsvängen 7 B, PB 1705 02044 VTT
tel. växel (09) 4561, fax (09) 456 7039

VTT Industrial Systems, Otakaari 7 B, P.O.Box 1705, FIN–02044 VTT, Finland
phone internat. + 358 9 4561, fax + 358 9 456 7039

Technical editing Leena Ukskoski

Otamedia Oy, Espoo 2003

Bäckström, Mika. Multiaxial fatigue life assessment of welds based on nominal and hot spot stresses. Espoo 2003. VTT Publications 502. 97 p. + app. 9 p.

Keywords fatigue life, assessments, nominal stresses, hot spot stresses, biaxial fatigue, multiaxial fatigue, welded joints, theses

Abstract

A little attention has been focused on multiaxial fatigue of welded joints, even though numerous industrial applications require the consideration of multiaxial effects. Therefore, the goal in present thesis was to find methods for fatigue assessment of welded joints in multiaxial loading cases. A survey of biaxial (bending or tension and torsion) constant amplitude fatigue test results of welded connections was also carried out. Re-analysis of these 233 experimental results from eight different studies was performed based on nominal and hot spot stresses. Three potential interaction equations and three damage parameters were used in the re-analysis.

The interaction equations were obtained from SFS 2378, Eurocode 3 and IIW recommendations. Of the three interaction equations SFS 2378 provided the least degree of scatter when design fatigue classes were used and with mean fatigue classes the IIW most successfully correlated the predicted and experimental lives.

Principal stress range, maximum shear stress range, and a modified critical plane model for welds were used as the damage parameters. The design hot spot S-N curves were FAT 84 for maximum principal stress range, FAT 109 for maximum shear stress range and FAT 97 for the modified critical plane model, when all toe failures were analysed with a slope of 3. However, observed scatter was 70–100% larger than that observed in uniaxial loaded specimens analysed using the hot spot approach.

Preface

Research work reported in this thesis was started in VTT Manufacturing Technology within a Nordic research project *Optimized Constructions Using High Strength Weldable Steels* (KONSPRO) and its Finnish part *Optimization of Weight and Endurance of Vehicle Structures* (NIRSO). NIRSO project was funded by National Technology Agency of Finland (Tekes), Nordic Industrial Fund (NI), Oy Närko AB, Rautaruukki Oy Metform, Patria Vehicles Oy and SISU Terminal Systems Inc. The research work was continued and completed within a *Mechanical Simulation & Fatigue* research project (ADAFAT) which was a part of *Improving Product Development Efficiency in Manufacturing Industries* research program (RAPID) and FATHTS *Fatigue based design rules for the application of high tensile steels in ships*. ADAFAT project was supported by Tekes, Tamrock Corporation, Patria Vehicles Oy and Valmet Automotive Inc.

The thesis work was directed by Professor Dr. Gary Marquis and advised by Dr. Aslak Siljander, to whom I would like to express my gratitude for their valuable comments and advice. I would like to thank the previewers of this thesis, Prof. Dr. Sonsino from Fraunhofer-Institute for Structural Durability (LBF) and Prof. Dr. Määttänen from Helsinki University of Technology, for their remarks and suggestions to the final manuscript. Professor emeritus Erkki Niemi, Mr. Mikko Lehtonen, Mr. Sauli Liukkonen and Mr. Asko Kähönen provided support and they were also a source for many helpful discussions.

A proportion of the text in the thesis has been presented in the *First North European Engineering and Science Conference, Fatigue Design 98 Symposium*, *Fatigue 2000* and *Sixth International Conference on Biaxial/Multiaxial Fatigue & Fracture* and other aspects has been published in the *Fatigue & Fracture of Engineering Materials & Structures* journal. Professor Dr. Gary Marquis, Dr. Aslak Siljander and Dr. T.P.J. Mikkola, in the above-mentioned publications, provided help in evaluating the testing and analysis results and in writing the texts. Special thanks for arranging the test specimens as co-authors are expressed to Mr. Reijo Ilvonen from Rautaruukki Corporate R&D, Hämeenlinna, and Mr. Oliver Ortmans, Chantiers de l'Atlantique. Tube-to-plate fatigue tests were performed by Mr. Risto Kuitunen, as co-author, and window corners by Mr. Juha

Juntunen. All analysis work presented in the thesis and all major conclusions are the work of the author as well as the most of the fatigue test supervision.

I wish to express my most sincere gratitude to Research Professor Dr. Matti K. Hakala, the Head of Maritime and Mechanical Engineering, Dr. Harri Soininen, the Head of Industrial Systems, Dr. Aslak Siljander, as Aircraft Structures group manager, and Mr. Asko Kähönen, as the Structural Integrity group manager, for the possibility to complete this thesis work during the office hours in between other research activities. Thanks are extended to Ms Marisa Lundström for her kind assistance in preparing the final manuscript.

Finally, I would like to thank my wife Satu and my daughters Sara and Sofie for their encouragement during the entire project.

Contents

List of symbols

$\Delta\sigma$, $\Delta\tau$	normal and shear stress range
$\Delta\sigma_1$, $\Delta\sigma_2$	maximum and minimum principal stress range
$\Delta\sigma_C$, $\Delta\tau_C$	alternating normal and shear stress range corresponding to $2 \cdot 10^6$ cycles
$\Delta\sigma_{eff}$	alternating effective stress range
$\Delta\tau'$	effective shear range
ΔK	stress intensity factor range
ε	strain
ϕ, θ	co-ordinate transformation angles
φ	angle between maximum principal stress and x-axis
ν	Poisson's ratio
σ, τ	normal and shear stress
σ_1, σ_2	maximum and minimum principal stress
σ_n	normal stress on a plane
σ_n^{max}	maximum value of normal stress on a plane during a load cycle
τ_f^*	constant of critical plane hot spot fatigue strength curve
A	co-ordinate system transform matrix
C	capacity
D	damage sum

E	modulus of elasticity
F, F_t	total actuator force in bending ($F = F_l + F_r$) and torsion ($F_t = - F_l + F_r$)
F_l, F_r	left and right actuator force
K_s	structural stress concentration factor
N	number of cycles
N_f	cycles to failure
N_{ref}	reference length of usage
R	stress ratio
W	section modulus
b	slope of stress-life curve
da/dN	crack growth per cycle
f	damage function, fatigue enhancement function
f_y	yield strength
k	material constant
l	lever arm of force
m	slope constant of fatigue strength curve
n_i	number of cycles at stress level i
s	standard deviation in log(C)
sN	standard error

Subscripts

I, II, III	deformation modes of cracks
σ	normal stress
τ	shear stress
a	stress amplitude
eq	equivalent
hs	hot spot stress
m	mean stress
max	maximum value of stress at a point
min	minimum value of stress at a point
nom	nominal stress
s	structural stress
t	torsion
x, y, z	specified co-ordinate system
x', y', z'	transformed co-ordinate system

Original features

The following features of this thesis are believed to be original:

1. The test data for 22 welded rectangular tube-to-plate components is presented. Tube-to-plate components were tested with constant amplitude bending only, torsion only and combined bending- torsion proportional and non-proportional loading. Rectangular tubes are often used in fatigue critical design and these tests compliment the more common circular tube data available from the literature.

2. A survey of biaxial (bending or tension and torsion) constant amplitude fatigue of welded connections is presented. Re-analysis of 233 experimental results from eight different studies has been performed based on hot spot stresses and three potential damage parameters: maximum principal stress range, maximum shear stress range, and a modified critical plane model for welds. In addition the experimental results have been evaluated based on three published interaction equations for nominal normal and shear stress. The interaction equations were obtained from SFS 2378, Eurocode 3 and IIW recommendations. Fatigue classes for normal and shear stress were obtained directly from the recommendations and they were determined also by baseline specimen data for bending only and torsion only loading.

3. A critical plane fatigue assessment criterion based on the Findley model is modified to be more suitable for welded structures. This is done by limiting the fatigue damage plane to be parallel to the weld toe and by considering residual stresses. The maximum principal stress range was also slightly modified so that only the changing portion of the stress during a loading event is used to compute the orientation. This was conducted so that the principal stress range was determined at each point in time during the cycle from the changes in stress component.

4. Full-scale window corners from a passenger ferry were also statically and fatigue tested. Bending-only proportional constant amplitude and spectrum loading was used. The stress state in the crack locations was biaxial.

These results have influenced the hot spot fatigue analysis procedures drafted by the International Institute of Welding for biaxial stress conditions.

5. Based on the re-evaluated data, design curve recommendations for the different analysis methods have been made.

1. Introduction

1.1 Fatigue of welded joints

In the context of engineering, fatigue is defined as a process of cycle by cycle accumulation of damage in a material undergoing fluctuating stresses and strains. A significant feature of fatigue is that the load is not large enough to cause immediate failure. Instead, failure occurs after a certain number of load fluctuations have been experienced (Almar-Naess 1985, Bannantine et al. 1990, Fuchs & Stephens 1980, Gurney 1979, Maddox 1991, SAE AE-10 1988).

The fatigue process can generally be broken into two distinct phases: initiation and propagation life of the crack (Bannantine et al. 1990). The initiation fatigue life is usually short in the welded structures because it can always be assumed that sharp-edged discontinuities exist in a welded structure (Almar-Naess 1985, Maddox 1991, Nykänen 1993, PD 6493 1991, SFS 2378 1992). According to the existence of discontinuities, the fatigue life estimations for welded structures are often based on the fatigue life propagation using fracture mechanics (Almar-Naess 1985, Niemi 1995). The crack growth rate is approximately the same for all weldable structural steels, regardless of the yield limit of the material. Thus, the same fatigue strength curves can be applied to different weldable structural steels (Almar-Naess 1985, Maddox 1991).

Most welded structures are in the as-welded condition and contain welding-induced tensile residual stresses of the order of the yield strength of the material. This means that the mean stresses have a minimal effect on the fatigue strength of welded joints and the fatigue failure can occur in welded joints under nominally compressive stresses (Almar-Naess 1985, SFS 2378 1992, Maddox 1991). Stress range seems to be the main controlling parameter of the fatigue strength of the welded structures (Almar-Naess 1985, Gurney 1979, Maddox 1991, Niemi 1995).

Most service loading histories are variable amplitude and can be quite complex. Linear damage rules and non-linear damage theories have been developed to deal with variable amplitude loading using the baseline data generated from constant amplitude tests. The linear damage rule was first proposed by Palmgren

in 1924 and was further developed by Miner in 1945. Today this method is commonly known as Miner's rule or Miner-Palmgren formula. Main shortcoming with the Miner's rule is that the damage of load cycle is assumed to be independent of where it occurs in the load history (Almar-Naess 1985, Bannantine et al. 1990).

A recent study by Fatemi & Yang (1998) reported a survey of more than 50 damage rules developed between the early 1970s to the early 1990s. They concluded that none of these damage models enjoys universal acceptance. After all Miner's rule gives quite acceptable estimations of fatigue life and it is simply to use in most practical instances with real measured signals. Hence, many standards are based on Miner's rule.

Structural design codes (Eurocode 3 1992, IIW recommendations by Hobbacher 1996, SFS 2378 1992) for the fatigue of welds normally rely on the nominal stress approach in which different weld geometries are assigned strength values based on constant amplitude laboratory fatigue tests. Weld details are then grouped into classes having similar fatigue life endurance properties (Almar-Naess 1985, Marquis 1995).

Hot spot stress approach is in an area of growing interest to fatigue design for plated as well as tubular structures (Partanen & Niemi 1996). The hot spot approach is generally based on strains measured in the specimen near the point of crack initiation. The fatigue life of different weldments are estimated using a single S-N curve where cycles to failure is presented as a function of hot spot stress range. One advantage of the hot spot stress approach is the possibility of predicting the fatigue lives of many types of joints configuration using a single S-N curve (Eurocode 3 1992, IIW recommendations by Hobbacher 1996, Marquis 1995, Niemi 1995).

The high cycle fatigue research has an increasing interest for welded joints. The fatigue design standards for welded joints are using Miner's rule in conjunction with a modified endurance (S-N) curve to allow the damaging effect of stresses below the constant amplitude fatigue limit. There is growing evidence that the current approach may be unsafe particularly in the long-life regime. Marquis (1995) has proposed that for long-life regime a straight line extension of the S-N

curve below the fatigue limit using a slope of 3, best fits the data for fatigue tests as long as $2 \cdot 10^7$ cycles to failure for welded components.

1.2 Fatigue of structural hollow sections

Circular and rectangular hollow sections are widely used in the offshore structures, road bridges, railway bridges, cranes, slender elements (wind induced vibrations) and the field of mechanical applications. Tubular members are usually connected by some form of welded joint. Welded hollow section connections are very economic because they need no gussets or stiffening plates (Dutta et al. 1996, Wardenier et al. 1995, Zhang 1994).

There are generally three kinds of mechanical failures in structural components and welded tubular joints: stability, plastic collapse and fatigue. (Dutta et al. 1996, Wardenier et al. 1995, Zhang 1994). The fatigue behaviour of hollow sections is largely influenced by the loading, plate thickness and the way the members are connected. The stress distribution is non-uniform due to the non-uniform stiffness around the welded intersection of hollow section connections. This non-uniform stress distribution depends on the type of loading, the connection types and geometry. It can be axial or bending in plane and out of plane. This is the reason why the welded hollow section connections have to be treated in a different way than the welded connections between plates in the fatigue assessment (Dutta et al. 1996, Wardenier et al. 1995, Wingerde 1992).

1.3 Review of the methods for multiaxial fatigue

1.3.1 Stress, strain and energy based models

Many engineering components such as crankshafts, propeller shaft, and axles are subjected to complex states of stress and strain. The complex stress states in which the two or three principal stresses are proportional or non-proportional often occur at geometric discontinuities e.g. notches or joints connections. Fatigue under these conditions, termed as multiaxial fatigue, is an important design

consideration for reliable operation and optimisation of many engineering components (Bannantine et al. 1990, SAE AE-14 1989, Socie & Marquis 2000).

During the last 50 years many stress and strain based multiaxial theories have been developed. A comprehensive presentation of these theories has been done by Socie & Marquis (2000). The strain-based methods are typically associated with low cycle fatigue and the stress based methods with high cycle fatigue.

The early development of multiaxial fatigue theories was based on extension of static yield theories. One of these theories was published by Sines in 1955. Sines' multiaxial theory was very similar to the von Mises' static yield theory but included a hydrostatic term. Several theories were developed from Sines' approach. These empirical models can be made to fit some of the available data by inclusion of suitable constants, but are incapable of capturing the complex load interactions often observed in more general multiaxial fatigue loading.

The most successful stress based theories use the critical plane models. The critical plane models have largely developed from observations of fatigue cracking behaviour of smooth specimens, which show that cracks initiate and propagate in preferential orientations. One of the first critical plane fatigue damage models was developed by Findley (1959) and is based on the alternating shear stress modified by the normal stress on the plane of failure. Further, Brown and Miller (1973) reviewed the available data on multiaxial fatigue and emphasised the importance of the plane orientation for early crack growth. They noted that an appropriate damage model should relate the observed cracking behaviour with strain components acting on the planes of cracking.

1.3.2 Fracture mechanics

The deformation of the cracks is usually divided in three basic modes shown in Figure 1. These modes of the deformation are usually referred to simply by roman numerals I, II and III. Other descriptions used are opening mode or tension mode for mode I, in-plane shear for mode II and out-of-plane shear for mode III. In practice, the majority of macroscopic cracks are generally assumed to result from mode I. Pure mode II and III propagation of cracks is rarely observed but these modes often act in combination with mode I. However, if the loading of

these modes is in phase, cracks will rapidly choose a direction of growth in which they are subjected to mode I. Thus, the majority of apparent combined mode cases are reduced to mode I by nature itself (Broek 1988, Paris & Erdogan 1963, Socie & Marquis 2000).

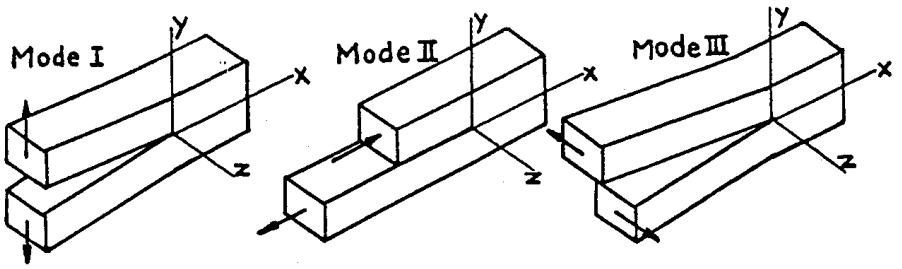

Figure 1. The basic modes of crack surface displacements (Paris & Erdogan 1963).

Schematic description of relationship between the rate of crack growth and the stress intensity factor in deformation mode I is shown in Figure 2. Yu et al. (1998) have pointed out that in deformation mode III the friction forces play a major role in the determination of the crack growth rate because the fracture surfaces are irregularly shaped. Further the material parameter data for modes II and III are rare because there are no standard test methods available. This makes comparison of data from different sources difficult (Pook 1994, Pook & Grawford 1991, Ritchie et al. 1982 and Yu et al. 1998).

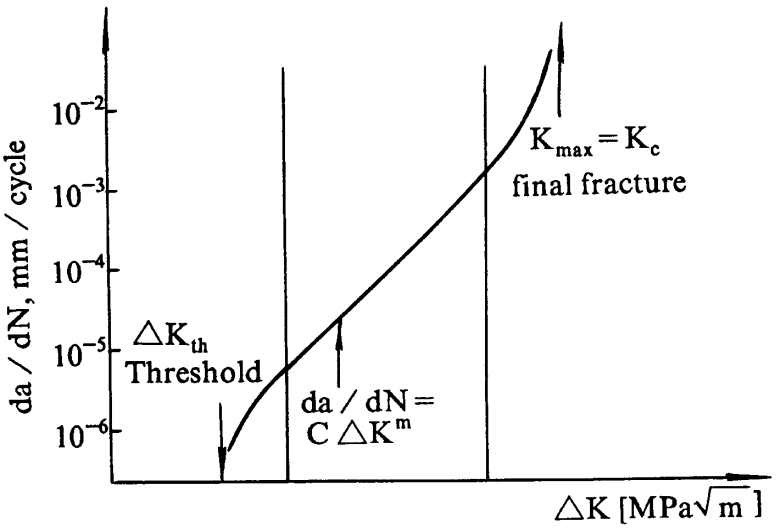

Figure 2. Schematic description of relationship between the rate of crack growth and the stress intensity factor in deformation mode I (Zheng 1994).

A simple power law is probably the most widely accepted method for describing the crack growth in constant or variable amplitude loading. This power law relationship between the rate of the crack growth per cycle (da/dN) and the range of stress intensity factor (ΔK_I) has been developed by Paris & Erdogan (1963), see Eq. (1).

$$\frac{da}{dN} = C\,(\Delta K_I)^m \qquad (1)$$

Growth rates for the cracks in multiaxial loading may be determined by using an equivalent stress intensity range. These equivalent stress intensity ranges are based e.g. on crack tip displacements Eq. (2) or strain energy release rate Eq. (3). The fatigue assessments are then conducted with Paris type equation by replacing ΔK_I with ΔK_{eq} (Socie & Marquis 2000).

$$\Delta K_{eq} = \left(\Delta K_I^4 + 8 \cdot \Delta K_{II}^4 + \frac{8 \cdot \Delta K_{III}^4}{1-\nu} \right)^{0.25} \qquad (2)$$

$$\Delta K_{eq} = \left(\Delta K_I^2 + \Delta K_{II}^2 + (1+\nu)\cdot \Delta K_{III}^2\right)^{0.5} \qquad (3)$$

Stress intensity factors for welds for deformation mode I can be found from literature. There is also weight functions to estimate the SIFs, because the stresses are not equal distributed through the plate thickness. The most modern way to solve the stress intensity factors are Finite Element (FE) or Boundary Element (BE) software. Automatic meshing during the crack growth is included in some software. The main problem using this type of software is that the simulation of the crack growth is very time consuming.

The meshing algorithm is more simple for BE-meshing than for FE-meshing. The main problem using BE-method is that the engineers are not familiar with this method and that the solving of the BE-model is not as fast as the FE-method (Becker 1992). In addition, if good results will be reached with BE-method a quite fine mesh is needed near the crack tip.

1.3.3 Damage maps

An important contribution to understanding multiaxial fatigue has been the development of damage maps. The main idea of the damage maps is to find out which kind of hypothesis it should be used in the fatigue assessment of different stage of crack growth. Socie (1993) and Socie & Furman (1996) have shown that the fatigue damage accumulation process consists of crack nucleation within a grain, crack arrest at a grain boundary, crack coalescence and shear crack nucleation, which is followed by crack growth on planes of maximum principal strain. This means that damage mechanism will change during the crack growth. An example of cracking behaviour in 1045 steel in torsion and tension is shown in Figure 3a and Figure 3b (Socie & Marquis 2000).

Figure 4 shows how damage accumulates in the fatigue process according to Miller (2000). He has concluded that damage is unambiguously related to crack length (a) and the rate of damage accumulation is therefore da/dN. He has also pointed out that different forms of fracture mechanics (linear elastic, elastic-plastic and microstructural fracture mechanics) are required to describe the growth behaviour. Figure 4 also shows that cracks of a given size will not grow

unless a sufficiently high stress is applied, microstructurally small cracks can grow and arrest, and there are three distinct zones for crack growth. One zone is applicable to large structures (a > 0.5–1 mm), one to components (a < 0.5 mm), and one to ground and polished laboratory specimens (a < 2 or 3 microns).

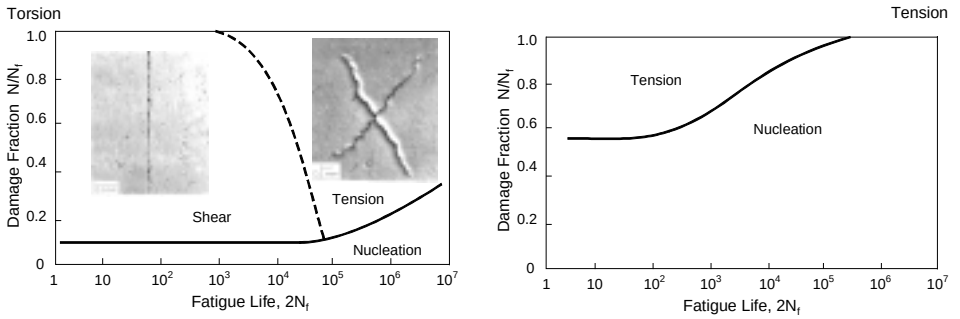

a) *b)*

Figure 3. Cracking behaviour observed in 1045 steel in a) torsion and b) tension (Socie & Marquis 2000).

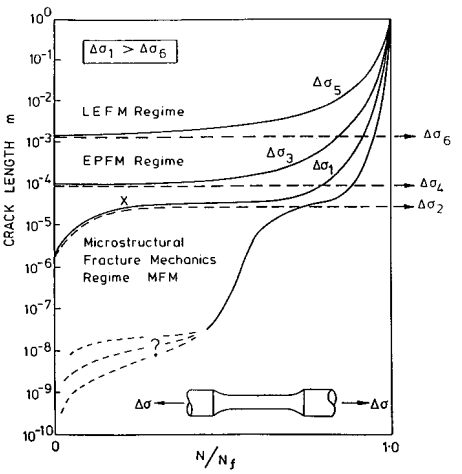

Figure 4. Fundamental crack growth behaviour patterns and three (possibly four) different zones of fracture mechanics characterisation (Miller 2000).

1.4 Purpose and scope

A little attention has been focused on multiaxial fatigue of welded joints, even though numerous industrial applications require the consideration of multiaxial effects. Therefore, a goal in present thesis was to find methods for fatigue assessment of welded joints in multiaxial loading cases. This study included fatigue tests, literature survey, comparison and evaluation of different standard methods, and development of a critical plane model suitable for fatigue assessment of welded joints.

This thesis is divided into six chapters. Following this first introduction chapter, chapter two presents methods used in the multiaxial fatigue assessment of welded joints. Data published in the open literature and the fatigue test results generated as parts of this thesis are presented in the third chapter. The multiaxial fatigue tests were conducted on a square hollow section tube-to-plate joint. The geometry was chosen so that it represented a typical joint type and material thickness employed in the vehicle structures in Finland. The non-proportional multiaxial loading histories were gathered from typical duty-cycle events from field measurements for the vehicle structures in Finland. In these field measurements the ratio between nominal normal and shear stress range was over 15%. According to the standards for welded structures, the combined effects of normal and shear stresses should be considered.

Re-analysis of the literature review and the fatigue test results are shown in the fourth chapter. The test results were correlated with various interaction equations and multiaxial fatigue damage parameters based on nominal and hot spot stresses. A discussion of fatigue tests and re-analysis results is given in the fifth chapter. Summary and conclusions of the work are presented in the last chapter.

The scope of this thesis is limited to biaxial and multiaxial fatigue of welded structures with weld toe failures. Emphasis is given to life region from 10^4 cycles to $2 \cdot 10^6$ cycles. In the re-analysis work and methods modification the nominal and the hot spot stresses are used instead of the local stresses. The modification of the analysis methods is limited to make the critical plane approach more suitable for welded structures. The evaluation of design codes is restricted to SFS 2378, Eurocode 3 and IIW recommendations.

2. Fatigue analysis

2.1 Stresses

2.1.1 State of stress

To understand fatigue it is essential to understand the state of stress of a component. Stress at a point in a component can be resolved onto an infinite number of planes passing through the point. This stress can be resolved into two components: a normal stress σ perpendicular to the area and a shearing stress τ acting in the plane of the area. One symbol is needed to denote the normal component of stress and two more symbols to denote the two components of shearing stress for each pair of parallel sides of a cubic element (Figure 5a*)*. To describe the stresses acting on the six sides of the element three symbols σ_x, σ_y and σ_z are necessary for normal stresses and six symbols τ_{xy}, τ_{yx}, τ_{xz}, τ_{zx}, τ_{yz} and τ_{zy} for shearing stresses. By a simple consideration of the equilibrium of the element, the number of symbols for shearing stresses can be reduced to three. The six quantities σ_x, σ_y, σ_z, $\tau_{xy} = \tau_{yx}$, $\tau_{xz} = \tau_{zx}$ and $\tau_{yz} = \tau_{zy}$ are therefore sufficient to describe the stresses acting on the co-ordinate planes through a point (Timoshenko & Goodier 1982).

The normal stress is taken positive when it produces tension and negative when it produces compression. The positive directions of the components of shear stress on any side of the cubic element are taken as the positive directions of the co-ordinate axes, if a tensile stress on the same side would have the positive direction of the corresponding axis. If the tensile stress has a direction opposite to the positive axis, the positive directions of the shear stress components should be reversed (Timoshenko & Goodier 1982). Positive directions of normal and shear stress are shown in Figure 5a.

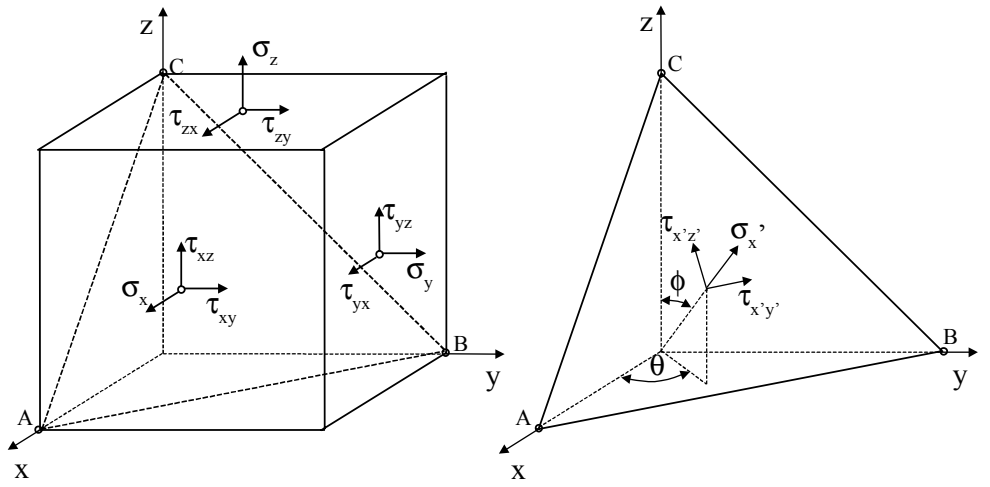

Figure 5. a) Stress components needed to describe the stress state at a point and b) stresses acting on a plane in a three dimensional co-ordinate system.

Stress state at a point is completely known, if the stress components in the Figure 5a is known. The oblique plane's normal and tangential stress components in the Figure 5b can be calculated from Eq. (4) to (7), when the stress components and the co-ordinate system transform matrix [A] is known. The resultant of two shear stresses on oblique plane (Figure 5b) can be resolved using Eq. (8).

$$\begin{bmatrix} a_{11} & a_{12} & a_{13} \\ a_{21} & a_{22} & a_{23} \\ a_{31} & a_{32} & a_{33} \end{bmatrix} = \begin{bmatrix} \cos\theta \cdot \sin\phi & -\sin\theta & -\cos\theta \cdot \cos\phi \\ \sin\theta \cdot \sin\phi & \cos\theta & -\sin\theta \cdot \cos\phi \\ \cos\phi & 0 & \sin\phi \end{bmatrix} \qquad (4)$$

$$\begin{aligned} \sigma_{x'} &= \sigma_x \cdot a_{11}^2 + \sigma_y \cdot a_{21}^2 + \sigma_z \cdot a_{31}^2 \\ &+ 2 \cdot \left(\tau_{xy} \cdot a_{11} \cdot a_{21} + \tau_{xz} \cdot a_{11} \cdot a_{31} + \tau_{yz} \cdot a_{31} \cdot a_{21} \right) \end{aligned} \qquad (5)$$

$$\begin{aligned}\tau_{x'y'} &= \sigma_x \cdot a_{11} \cdot a_{12} + \sigma_y \cdot a_{21} \cdot a_{22} + \sigma_z \cdot a_{31} \cdot a_{32} \\ &+ \tau_{xy} \cdot (a_{11} \cdot a_{22} + a_{21} \cdot a_{12}) + \tau_{yz} \cdot (a_{21} \cdot a_{32} + a_{31} \cdot a_{22}) \\ &+ \tau_{zx} \cdot (a_{31} \cdot a_{12} + a_{11} \cdot a_{32})\end{aligned} \tag{6}$$

$$\begin{aligned}\tau_{x'z'} &= \sigma_x \cdot a_{11} \cdot a_{13} + \sigma_y \cdot a_{21} \cdot a_{23} + \sigma_z \cdot a_{31} \cdot a_{33} \\ &+ \tau_{xy} \cdot (a_{11} \cdot a_{23} + a_{21} \cdot a_{13}) + \tau_{yz} \cdot (a_{21} \cdot a_{33} + a_{31} \cdot a_{23}) \\ &+ \tau_{zx} \cdot (a_{31} \cdot a_{13} + a_{11} \cdot a_{33})\end{aligned} \tag{7}$$

$$\tau' = \sqrt{\tau_{x'y'}^2 + \tau_{x'z'}^2} \tag{8}$$

2.1.2 Principal stresses

Knowing the stress components σ_x, σ_y and τ_{xy} at any point of a plate in a condition of plane stress, the maximum principal stresses can be determined from Eq. (9). The angle (φ) between the maximum principal stress and x-axis can be defined with Eq. (10).

$$\begin{aligned}\sigma_1 &= \frac{\sigma_x + \sigma_y}{2} + \sqrt{\left(\frac{\sigma_x - \sigma_y}{2}\right)^2 + \tau_{xy}^2}, \quad \alpha = \varphi \\ \sigma_2 &= \frac{\sigma_x + \sigma_y}{2} - \sqrt{\left(\frac{\sigma_x - \sigma_y}{2}\right)^2 + \tau_{xy}^2}, \quad \alpha = \varphi + \frac{\pi}{2}\end{aligned} \tag{9}$$

$$\begin{aligned}\tan 2\varphi &= \frac{2\tau_{xy}}{\sigma_x - \sigma_y} \\ \tau_{xy} \sin 2\varphi &\geq 0\end{aligned} \tag{10}$$

Figure 6 is an example of the proportional fatigue loading and Figure 7 of non-proportional. In both figures the normal and shear stress range is 100 MPa and the mean stresses are 50 MPa for normal stress and 0 MPa for shear stress. The phase shift between the normal and shear stress was 0° for proportional loading and 90° for non-proportional.

Left side diagrams in Figure 6 and Figure 7 are time histories for normal (σ) and shear stress (τ), maximum (σ_1) and minimum principal stress (σ_2), and maximum ($\Delta\sigma_1$) and minimum principal stress range ($\Delta\sigma_2$). Maximum principal stress range is determined from the maximum changes in the stress components during the loading event. This means that the principal stress range is determined at each point in time during the cycle from the changes in stress component. Start point was the point in the time history where maximum principal stress gets its maximum value as shown in Figure 6.

Right side diagrams in Figure 6 and Figure 7 present the relation between normal and shear stress (σ-τ), maximum and minimum principal stress (σ_1-σ_2), and maximum and minimum principal stress range ($\Delta\sigma_1$-$\Delta\sigma_2$). It is interesting to note that for proportional loading (Figure 6) the direction between the minimum and maximum principal stress range is constant which means that the relation between the principal stress range ($\Delta\sigma_1$-$\Delta\sigma_2$) is proportional. However, the direction of principal stress varies during the load cycle causing a non-proportional ratio between the maximum and minimum principal stress (σ_1-σ_2). For non-proportional loading the direction and relation between maximum and minimum stress and stress range varies (Figure 7, σ_1-σ_2 and $\Delta\sigma_1$-$\Delta\sigma_2$).

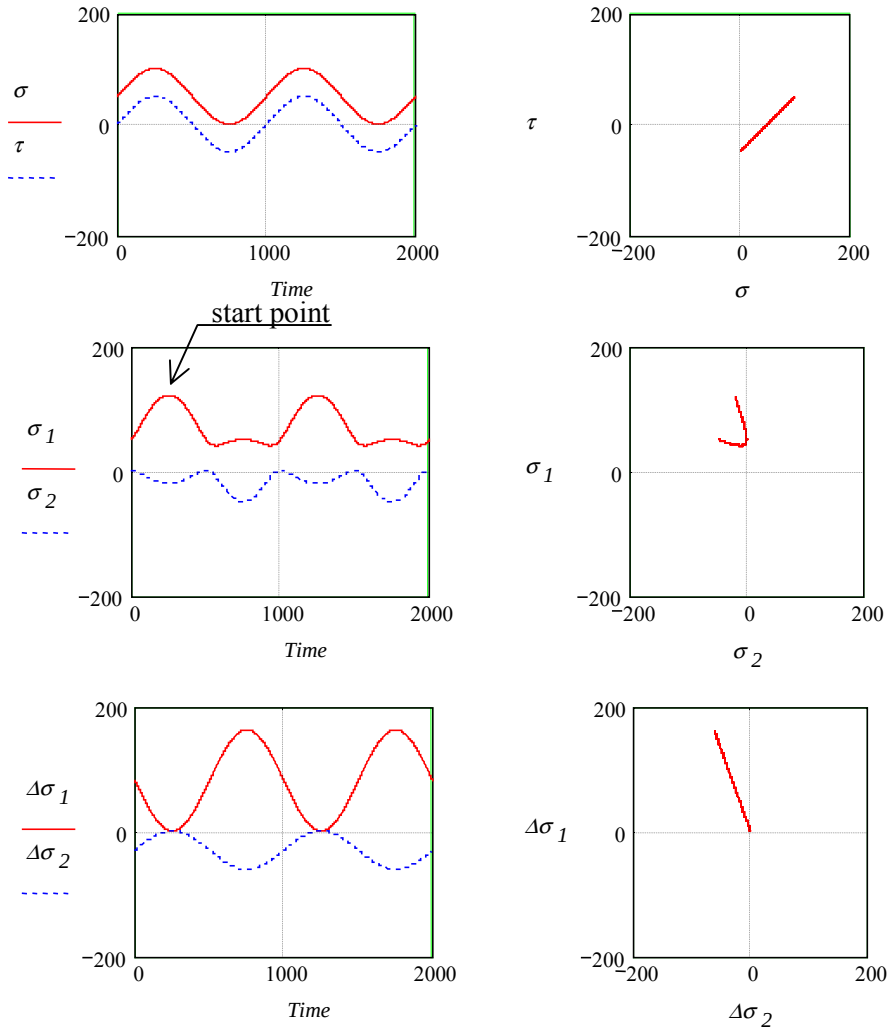

Figure 6. Six diagrams to clarify proportional biaxial stress state in fatigue loaded component. Left side diagrams are time histories for normal and shear stress, maximum and minimum principal stress, and maximum and minimum principal stress range. Right side diagrams present the relation between normal and shear stress, maximum and minimum principal stress, and maximum and minimum principal stress range.

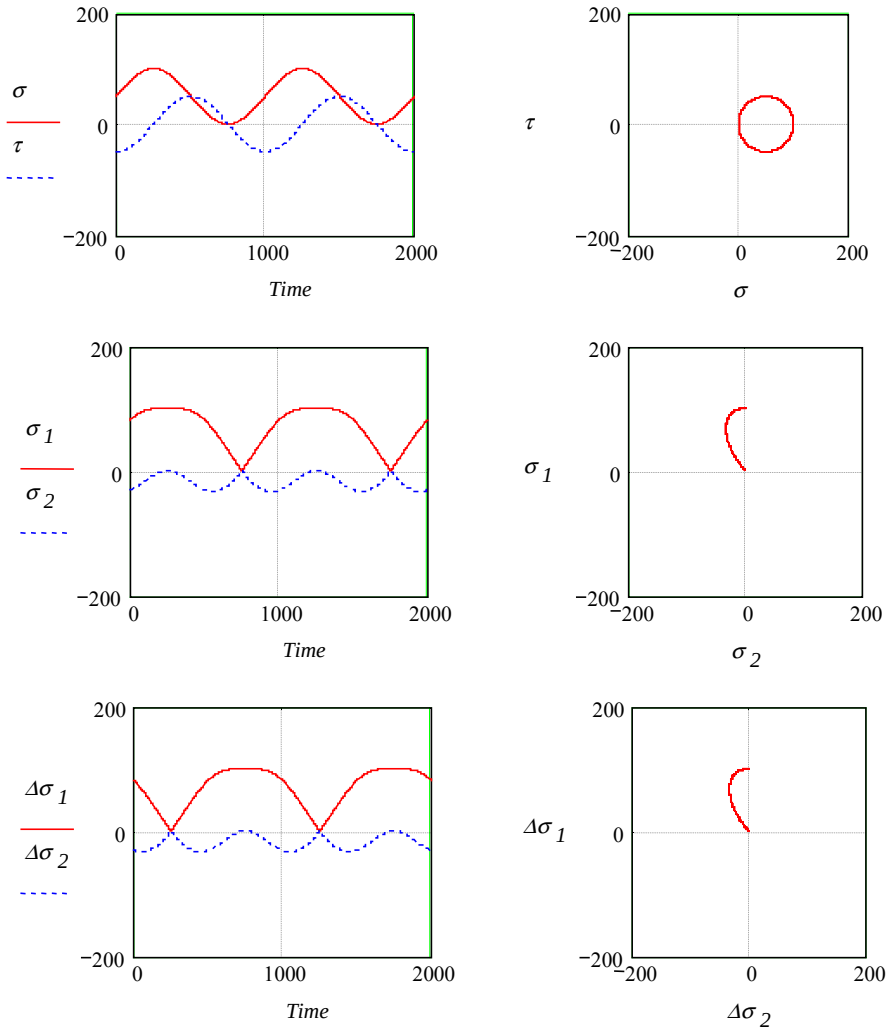

Figure 7. Six diagrams to clarify non-proportional biaxial stress state in fatigue loaded component. Left side diagrams are time histories for normal and shear stress, maximum and minimum principal stress, and maximum and minimum principal stress range. Right side diagrams present the relation between normal and shear stress, maximum and minimum principal stress, and maximum and minimum principal stress range.

2.2 Fatigue loading

Static stresses are residual stresses and stresses caused by permanent loads. In a structure exhibiting linear behaviour they do not contribute to the stress range, which is the difference between the maximum and minimum stresses (Figure 8). Permanent loads need to be taken into account in the stress range calculation only in those cases in which the deformations of the structure are large enough to cause geometrically non-linear behaviour (Niemi 1995).

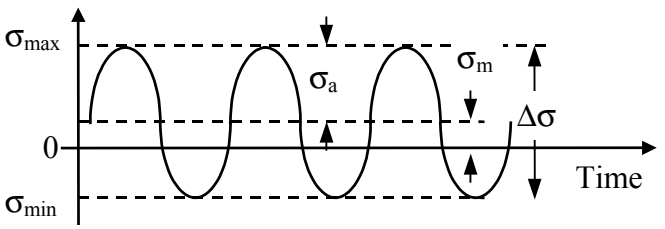

Figure 8. Terminology used to describe constant amplitude fluctuating stress.

Some fatigue analysis methods take into account the effect of mean stress (σ_m) or the stress ratio (Niemi 1995). The stress ratio can be determined for normal (R) and shear stress (R_τ) from Eq. (11). Generally, the mean stress and stress amplitude are used with crack initiation when stress range and stress ratio is applied to crack growth calculations.

$$R = \frac{\sigma_{\min}}{\sigma_{\max}} \qquad R_\tau = \frac{\tau_{\min}}{\tau_{\max}} \tag{11}$$

2.3 Nominal stress approach

2.3.1 Basis of rules

Design rules for welded structures are based on a statistical analysis of fatigue test results of welded joints (Eurocode 3 1992, SFS 2378 1992, IIW recommendations by Hobbacher 1996). The welded joints are classified in fatigue classes (FAT), which are identified with the characteristic fatigue strength value at the stress cycle number $N = 2 \cdot 10^6$. The characteristic fatigue strength is generally two standard deviations below the mean. This means that the characteristic fatigue strength is a value that indicates the magnitude of loading at which 2.3% of the test specimens fails.

In the design rules nominal normal ($\Delta\sigma_{nom}$) and shear ($\Delta\tau_{nom}$) stress ranges are calculated using the theory of elasticity. In fatigue design each part of the welded joints must be placed into one of fatigue classes. The classification of the joints varies slightly in different rules. For each fatigue class the relation between applied stress range and fatigue life can be written

$$N \cdot \Delta\sigma_{nom}{}^{m} = C \tag{12}$$

$$N \cdot \Delta\tau_{nom}{}^{m_\tau} = C_\tau \tag{13}$$

$$\begin{aligned} C &= FAT^{m} \cdot 2 \cdot 10^6 \\ C_\tau &= FAT^{m_\tau} \cdot 2 \cdot 10^6 \end{aligned} \tag{14}$$

For spectrum loading it is not practical to read the allowable stress ranges directly from curves on logarithmic scale (Figure 9). For this reason, some standards use equivalent stress range instead of the true stress spectrum. The equivalent stress range is normalised with N_{ref} stress cycles, see Eq. (15) and (16). For example, Niemi (1996) has described application of the equivalent stress range.

$$\Delta\sigma_{eq.nom} = \sqrt[m]{\frac{\sum_{i=1}^{k}\left(\Delta\sigma_{nom\ i}{}^{m} \cdot n_i\right)}{N_{ref}}} \qquad (15)$$

$$\Delta\tau_{eq.nom} = \sqrt[m_\tau]{\frac{\sum_{i=1}^{k}\left(\Delta\tau_{nom\ i}{}^{m_\tau} \cdot n_i\right)}{N_{ref}}} \qquad (16)$$

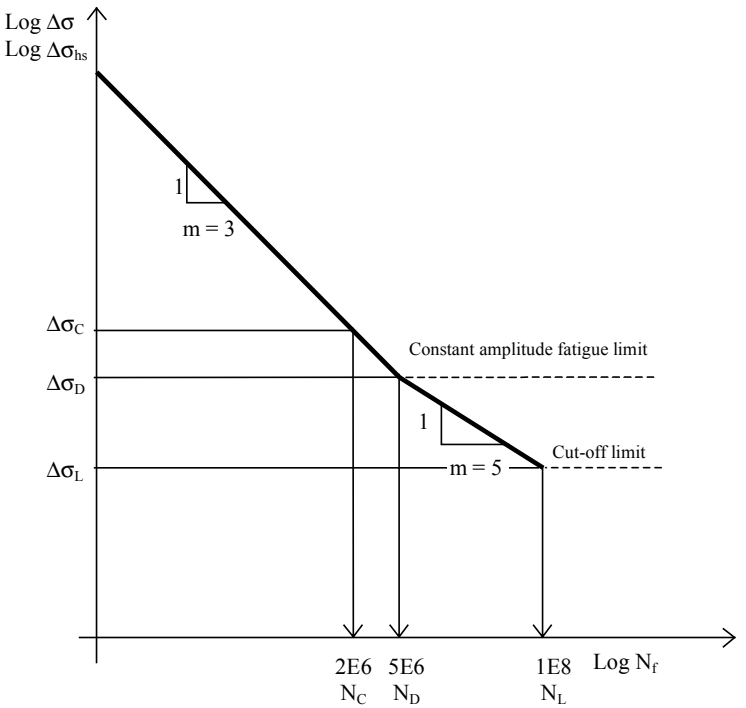

Figure 9. Fatigue strength curve for welded joints.

For stress relieved welded details SFS 2378 (1992) and Eurocode 3 (1992) suggest that the compressive portion of normal stress range can be reduced to 60%. IIW recommendations (Hobbacher 1996) has defined that the fatigue class should be multiplied by a fatigue enhancement factor f(R). For the stress re-

lieved components with residual stresses less than 0.2 · fy the fatigue enhancement factor is:

$$\begin{aligned} f(R) &= 1.6 && for R < -1 \\ f(R) &= -0.4 \cdot R + 1.2 && for\ -1 \le R \le 0.5 \\ f(R) &= 1 && for\ R > 0.5 \end{aligned} \qquad (17)$$

2.3.2 SFS 2378

SFS 2378 (1992) standard is based on fatigue strength curves presented by International Institute of Welding (IIW). All curves have a slope of m = m_τ = 3 in a double logarithmic scale down to a constant amplitude fatigue limit (Figure 9).

Usually several stress components occur simultaneously in structural components. The direction of the principal stresses may be fixed (proportional) or vary during the loading cycles (non-proportional). In each case, the factor of utilisation of every stress component is checked separately and their interaction calculated as follows (SFS 2378 1992):

$$\frac{\Delta\sigma_{eq.nom}}{\Delta\sigma_C} \le 1 \qquad (18)$$

$$\frac{\Delta\tau_{eq.nom}}{\Delta\tau_C} \le 1 \qquad (19)$$

$$\left(\frac{\Delta\sigma_{eq.nom}}{\Delta\sigma_C}\right)^2 + \left(\frac{\Delta\tau_{eq.nom}}{\Delta\tau_C}\right)^2 \le \left(\frac{1}{0.9}\right)^2 = 1.23 \qquad (20)$$

Eq. (20) is written using equivalent stress ranges for normal and shear stresses. The equivalent stress ranges can be replaced with Eq. (15) and (16) which leads to following damage criterion:

$$D_\sigma \le 1$$

$$D_\tau \le 1 \qquad (21)$$

$$D_\sigma^{\frac{2}{3}} + D_\tau^{\frac{2}{3}} \le 1.23$$

2.3.3 Eurocode 3 and IIW recommendations

The fatigue strength curves for normal stresses are double slope curves with two slope constants m = 3 and m = 5 as shown in Figure 9. Both standards also define two shear stress fatigue strength curves which follow a slope of $m_\tau = 5$ over the entire life regime to a cut-off limit of 10^8 cycles. The fatigue strength curve of FAT 100 is used for full penetration butt welds and FAT 80 for fillet and partial penetration butt welds in shear (Eurocode 3 1992 and IIW recommendations by Hobbacher 1996).

In the case of a combination of normal and shear stresses, the fatigue assessment shall consider their combined effects. There is three different alternatives in Eurocode 3 (1992):

1. The effects of the shear stress range may be neglected, if the equivalent nominal shear stress range in Eq. (16) is less than 15% of the equivalent nominal normal stress range in Eq. (15).

2. The maximum principal stress range may be used at locations other than weld throats, if the plane of the maximum principal stress does not change significantly in the course of a loading event (proportional loading).

3. For non-proportional loading events, the components of damage for normal and shear stresses shall be assessed separately using the interaction Eq. (22) or the Palmgren-Miner rule shown in Eq. (23). The equivalent stress range for nominal normal and shear stress is calculated from Eq. (15) and (16).

$$\left(\frac{\Delta\sigma_{eq,nom}}{\Delta\sigma_C}\right)^3 + \left(\frac{\Delta\tau_{eq,nom}}{\Delta\tau_C}\right)^5 \le 1 \qquad (22)$$

$$D_\sigma + D_\tau \leq 1 \qquad (23)$$

Four alternative design situations involving combined shear and normal stresses are defined by IIW recommendations (Hobbacher 1996):

1. The effects of the shear stress range may be neglected, if the equivalent nominal shear stress range is less than 15% of the equivalent nominal normal stress range or the damage sum of shear stress range is less than 10 % of the normal stress.

2. The maximum principal stress range may be used, if the plane of the maximum principal stress does not change significantly in the course of a loading event (proportional loading).

3. For non-proportional loading events, the components of damage for normal and shear stresses shall be assessed separately by using the interaction Eq. (22) or the Palmgren-Miner rule shown in Eq. (23). The usage of 0.5 of the calculated life cycles or the Palmgren-Miner damage sum of $\Sigma D_i = 0.5$ is recommended.

4. Fracture mechanics crack propagation calculations should be based on a maximum principal stress range.

2.4 Hot spot approach

2.4.1 Hot spot stress and structural stress concentration factor

Hot spot is a term, which is used to refer to the critical point in a structure, where fatigue cracking can be expected to occur due to a discontinuity and/or a notch (Figure 10). Usually, the hot spot is located at the weld toe. The hot spot stress is the value of the structural stress at the hot spot (Niemi 1995). The hot spot stresses account only the overall geometry of the joint and exclude local stress concentration effects due to the weld geometry and discontinuities at the weld toe. As Figure 15 shows hot spot normal stress (σ_{hs}) in Eq. (24) and hot

spot shear stress (τ_{hs}) in Eq. (25) can be calculated using a linear extrapolation and the measured stresses at location $x_1 = 2.3$ and $x_2 = 9.8$.

$$\sigma_{hs} = \left(1 + \frac{x_1}{x_2 - x_1}\right) \cdot \sigma_s(x_1) - \left(\frac{x_1}{x_2 - x_1}\right) \cdot \sigma_s(x_2) \tag{24}$$

$$\tau_{hs} = \left(1 + \frac{x_1}{x_2 - x_1}\right) \cdot \tau_s(x_1) - \left(\frac{x_1}{x_2 - x_1}\right) \cdot \tau_s(x_2) \tag{25}$$

Structural stress concentration factor in bending ($K_{s.\sigma}$) and torsion ($K_{s.\tau}$) loading are:

$$K_{s.\sigma} = \frac{\sigma_{hs}}{\sigma_{nom}} \tag{26}$$

$$K_{s.\tau} = \frac{\tau_{hs}}{\tau_{nom}} \tag{27}$$

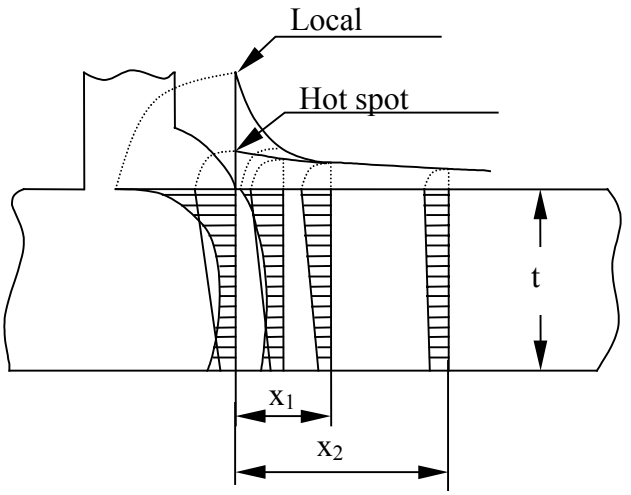

Figure 10. Stress distributions across the plate thickness and along the surface in the vicinity of a weld toe ($x_1 \approx 0.4 \cdot t$).

2.4.2 Hot spot SN curves

Hot spot SN curves are generally based on strains measured from various test specimens near the point of crack initiation. The strain ranges are measured with strain gauges at several sections along the weld toe and extrapolated to the weld toe from two or three strain measurement points. The hot spot SN curves can be presented using stress or strain ranges. Recently it is recommended that the hot spot fatigue analysis should be based on stress range (Niemi 1995).

LUT butt weld design curve is based on about 180 fatigue tests on arc welded steel joints (Partanen & Niemi 1996). The fatigue tests were carried out at Lappeenranta University of Technology (LUT) between 1980 and 1993. A mean fatigue strength of FAT 148 and characteristic fatigue strength of FAT 107 were obtained by considering all the specimens in one series. For toe failure of welded joints with plate thickness up to 10 mm, it is recommended that the fatigue class FAT 100 can be used as the design curve.

In Eurocode 3 (1992) the fatigue life estimation can be based on hot spot stress ranges. The hot spot stress is defined to be the maximum principal stress in the parent material adjacent to the weld toe. For full penetration butt welds two different hot spot curves are presented. FAT 90 is used, if weld profile and permitted weld defects acceptance criteria are satisfied and FAT 71 when only permitted weld defects acceptance criteria are satisfied.

IIW recommendations (Hobbacher 1996) defines different hot spot curves for butt welds, fillet welds and cruciform joints. Fatigue class of FAT 100 is used for fillet welds. Butt welds and cruciform joints are assessed according to their nominal fatigue classes.

2.5 Critical plane approach

Critical plane models have largely developed from observations of fatigue cracking behaviour of smooth specimens, which show that cracks initiate and propagate in preferential orientations. Brown and Miller (1973) reviewed the available data on multiaxial fatigue and emphasised the importance of the plane orientation for early crack growth. They noted that an appropriate damage model

should relate the observed cracking behaviour with strain components acting on the planes of cracking. In contrast to critical plane models are traditional multiaxial fatigue theories that are often extensions of multiaxial yield criteria. These empirical models can be made to fit some of the available data by the inclusion of suitable constants but are incapable of capturing the complex load interactions often observed in more general multiaxial fatigue loading. One of the first critical plane fatigue damage models was developed by Findley (1959) and it is based on the alternating shear stress modified by the normal stress on the plane of failure.

Findley suggested that the normal stress (σ_n) on a shear plane had a linear influence on the allowable alternating shear stress ($\Delta\tau/2$).

$$\frac{\Delta\tau}{2} + k\sigma_n = \frac{\Delta\tau'}{2} = f \qquad (28)$$

Any combination of $\Delta\tau$ and σ_n resulting in the same effective shear range ($\Delta\tau'$) gives the same fatigue life. The constant k represents a material's sensitivity to normal stress on a shear plane. Failure is expected to occur on the plane that has the largest $\Delta\tau'$ and not necessarily the plane of largest alternating shear stress. Often the superscript ^{max} is added to represent the maximum value of normal stress that occurs during a load cycle (σ_n^{max}).

Five modifications of the original Findley model were suggested by Marquis et al. (1997) to make it more suitable for welded structures.

1. In welded constructions, the vast majority of cracks are initiated along the weld toes where regions of high stress concentration and local geometric irregularities exist. Therefore, the critical damage plane is assumed to be a shear plane parallel to the line of the weld toe. Other planes are neglected.

2. Maximum normal stresses on a damage plane are computed by assuming yield strength magnitude stresses normal to the weld toe or, in the case of stress relieved joints, the maximum applied hot spot normal stress during the load spectrum. If the maximum applied stresses cause yielding at the hot spot, the maximum normal stress on the damage plane is computed based on the yield strength.

3. The hot spot technique documented by Niemi (1995) is used to estimate the local normal stress along the weld toe. Either strain gages or FEM analysis can be used to determine the normal hot spot stress concentration factors.

4. Stress gradients for shear are highly localised and cannot be effectively measured by using strain gage techniques. Hot spot stress estimates based on FEM are used for determining the shear stress along the weld toe.

5. The damage function (*f*) in Eq. (28) is assumed to be linear in a $\log(N_f)$ vs. $\log(\Delta\tau')$ plot.

$$\Delta\tau'_{hs} = \Delta\tau_{hs} + 2 \cdot k \cdot \sigma_{n.hs}^{\max} = \tau_f^* (N_f)^b \qquad (29)$$

where τ_{hs} is the hot spot shear stress and $\sigma_{n.hs}^{max}$ is maximum of either the yield strength of the material or, for stress relieved joints, the largest applied hot spot stress occurring during one application of the load cycle.

The first modification to the critical plane model for welds can be illustrated by considering the tube-to-plate weld shown in Figure 11 which is subject to bending and torsion loads as shown. The line of the weld toe in the region of highest stress is parallel to the y-axis and, therefore, the possible critical planes are limited to those being perpendicular to the x-z plane, i.e., $\theta = 0°$ as defined in Figure 11.

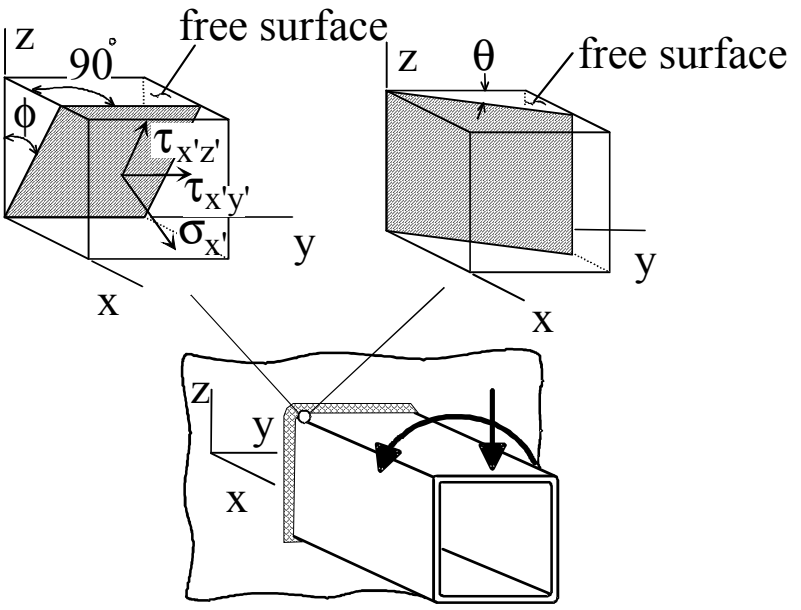

Figure 11. Damage plane orientation at the weld toe.

Also shown in this figure are the proposed potential critical planes. These comprise any plane oriented at an angle ϕ with respect to the y-z plane. For each load history, suitable co-ordinate transformation relations can be used to find the angle ϕ that represents the largest combination $\Delta\tau/2 + k\sigma_n^{max}$ during one cycle or, for more complex histories, during one repetition of the load history. Fatigue life for the component is computed using Eq. (29) for the plane of maximum damage. Different angles ϕ will be computed depending on the ratio of bending to torsion and the phase relationship. For complex multiaxial load histories, locating the plane experiencing maximum damage requires a search routine since it may change from cycle to cycle. However, it is usually sufficient to calculate damage on planes at 10° intervals since the damage on planes oriented ±5° from the critical plane will show virtually the same value of the damage parameter.

If the only two applied loads are σ_x due to bending and τ_{xy} due to torsion loads, it can be shown using appropriate co-ordinate transformation relations that the normal stress and shear stresses acting on a plane oriented ϕ are given as:

$$\sigma_{x'} = \sigma_x \cos^2 \phi$$

$$\tau_{x'y'} = \tau_{xy} \cos\phi \qquad (30)$$

$$\tau_{x'z'} = -\sigma_x \cos\phi \sin\phi$$

From these, the stress state on any plane can be computed throughout the load history. An example calculation for critical plane approach is shown in Appendix A.

2.6 Effective equivalent stress hypothesis (EESH)

Effective equivalent stress hypothesis was proposed by Sonsino (1997) because he has noted that neither the maximum principal stress criterion nor the von Mises criterion was relevant for non-proportional combined bending-torsion loading. His method assumes that cracks initiate by shear and involves calculating the interaction of all shear stress components in a surface- or volume-element at the weld toe. Stresses are calculated from the local strains and shear stresses at the weld toe. An example of application effective equivalent stress hypothesis is shown in Appendix B.

3. Fatigue data for welded joints

3.1 Literature review

3.1.1 General

Kouba & Stallmayer in 1959, Gurney & Woodley in 1962 and Braithwaite in 1964 were possibly the first researchers to address the question of biaxial fatigue of welded joints. According to Gurney (1979), tests were conducted with proportional loading for beams with fillet stiffeners welded to the web. It was concluded that fatigue lives were better correlated on the basis of maximum principal stress range rather than the uniaxial bending stress range. Archer (1987) and Siljander et al. (1992) were the first to consider the question of non-proportional loading of welded details. Siljander et al. found that non-proportional loading was more damaging than proportional loading while Archer found them to be equally damaging. An overview of the test series carried out by different researchers during the past 15 years is given in Table 1. While this table lists a total of 314 test data points, only the 233 points that produced weld toe failures are re-analyzed in this work. Weld root/throat failures are excluded from this thesis.

Table 1. An overview of the test series carried out by different researchers with plate thickness from 3 mm to 10 mm.

Test results	Specimen	Bending or Tension only	Torsion only	Bending/ Tension and torsion	Bending/ Tension and torsion
				Proportional	Non-proportional
	[No.]	[No.]	[No.]	[No.]	[No.]
Archer (1987)	27	1	10	5	11
Yung and Lawrence (1986)	18	5	2	11	0
Siljander et al. (1992)	40	10	10	10	10
Sonsino (1995, 1997) Tube-Tube	78	25	8	24	21
Sonsino (1995, 1997) Tube-to-plate	47	7	0	20	20
Razmjoo (1996)	29	7	8	7	7
Bäckström et al. (1997a)	22	5	4	9	4
Dahle et al. (1997)	53	6	22	21	4
Total	314	66	64	107	77

3.1.2 Test data

Yung & Lawrence (1986) performed biaxial fatigue tests on circular tube-to-plate welded specimens (Figure 12a). The specimens, 14 as welded and four stress-relieved, were fabricated from ASTM A519 cold-drawn seamless steel tube. These fatigue tests were conducted with bending only, torsion only and proportional bending-torsion loading. Stress ratios, $\sigma_{nom.min} / \sigma_{nom.max}$ and $\tau_{nom.min} / \tau_{nom.max}$, were -1 in all tests. The experimental nominal bending-to-shear stress ratios, $\sigma_{nom.max} / \tau_{nom.max}$, ranged from 1.7 to 2.9 in combined bending-torsion tests. A total of 18 specimens was tested and fatigue lives ranged from $1 \cdot 10^4$ to

$2 \cdot 10^6$ cycles. All specimens failed at the weld toe. Experimental data was correlated by using the amplitudes of local bending stress, local octahedral shear stress and local maximum principal stress. The best correlation of the test data was obtained when the shear stresses were included in the analysis.

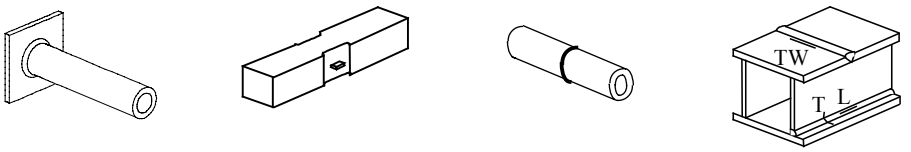

a) b) c) d)

Figure 12. Specimen geometry of a) circular tube-to-plate, b) box beams with longitudinal attachments, c) circular tube-to-tube, d) welded box beam (TW= crack in transverse weld, T = transverse crack, L = longitudinal crack).

Archer (1987) investigated the behaviour of structural box beams with two welded longitudinal attachments. Attachments were fillet welded to the webs of the box beams where the thickness had been reduced, Figure 12b. Specimens were made of BS4360 grade 43C steel and tested in the as-welded condition. Loading modes were bending, torsion and proportional and non-proportional combined bending-torsion. It should be noted that the phase difference in non-proportional tests was produced by using different frequencies for the bend and torsion loads. This leads to a cumulative damage problem, because smaller stress variations will be added to main cycle. The normal stress ratio was 0 or -1 and the shear stress ratio -1. Reported bending-to-torsion stress ratios ranged from 0.8 to 2.1 in the combined bending-torsion fatigue tests. A total of 27 specimens were tested. Fatigue lives ranged between $1 \cdot 10^5$ to $4 \cdot 10^6$ cycles and all specimens failed at the weld toe. Archer found that his fatigue test results were satisfactorily correlated using both an interaction equation approach and a "maximum damage" computational procedure. This analysis with the available limited experimental data suggested no pronounced difference between proportional and non-proportional loading.

Siljander et al. (1992) reported biaxial fatigue tests for circular tube-to-plate welded joints, Figure 12a, under proportional and non-proportional loading. Stress relieved specimens were fabricated from ASTM A519 cold-drawn seam-

less steel tube. Dimensions of Siljander's specimens were nearly identical to those of Yung and Lawrence. A total of 40 fatigue tests, bending only, torsion only and combined bending-torsion, were conducted. Fatigue lives ranged from $1 \cdot 10^4$ to $2 \cdot 10^6$ cycles. The bending stress ratio was 0 or -1 and the nominal bending-to-shear stress ratio was 1 to 7.4 in combined bending-torsion fatigue tests. All specimens failed at the weld toe. Test results were correlated by using various multiaxial fatigue damage parameters based on the local stresses. Local stresses at the weld toe were calculated with the FE-method. Siljander et al. found that the test results for both the proportional and non-proportional load histories were best correlated using Findley's equivalent shear stress model. It was noted that approximately 80% of the total fatigue life were spent in initiating the fatigue cracks.

Sonsino (1995, 1997) tested 47 circular tube-to-plate, Figure 12a, and 78 tube-to-tube joints, Figure 12c, with unmachined and machined welds. Bending only, torsion only and proportional and nonproportional combined bending-torsion loading were used in these tests. All tests were conducted at a stress ratio of -1 and the nominal bending-to-torsion ratio was 1.7 in the combined tension-torsion fatigue tests. Specimens were stress-relieved and failed at the weld toe. Fatigue lives ranged between $1 \cdot 10^4$ to $4 \cdot 10^6$ cycles. It was found that neither the maximum principal stress criterion nor the von Mises criterion was relevant for non-proportional combined bending-torsion loading. A new hypothesis for welded joints under multiaxial loading based on the effective equivalent stress (EESH) was proposed. This method assumes that cracks initiate by shear and involves calculating the interaction of all shear stress components in a surface- or volume-element at the weld toe. Stresses are calculated from the local strains and shear stresses at the weld toe.

Razmjoo (1996) investigated the fatigue performance of fillet welded tube-to-plate specimen, Figure 12a. Specimens were in the as-welded condition and tested under tension only, torsion only, and proportional and non-proportional combined tension-torsion loading. All tests were conducted at a stress ratio of zero. The nominal tension-to-shear stress ratio ranged from 0.33 to 2 in the combined tension-torsion fatigue tests. A total of 29 specimens were tested in the range of $1 \cdot 10^5$ to $1 \cdot 10^7$ cycles to failure. All cracks initiated at the weld toe in the tension only and the combined tension-torsion cases. Most of the specimens tested in torsion cracked at the weld throat. It was found that the maximum prin-

cipal stress range was a better criterion for proportional loading than the von Mises criterion. In the case of non-proportional loading, neither of the analysis methods was entirely satisfactory. Razjmoo suggested that the maximum principal stress range can be used for non-proportional loading with an extra safety factor of 1.7 when using the design S-N curves in BS 5400 or BS 7608.

Dahle et al. (1997) reported multiaxial fatigue test results on welded box beams, Figure 12d, which were fabricated of Domex 350 and Weldox 900 high strength steel. A total of 53 tests under bending only, torsion only and combined proportional and non-proportional bending-torsion loading, were performed. Fatigue lives ranged from $1 \cdot 10^4$ to $3 \cdot 10^6$ cycles. Stress ratios were -1 or 0 and the nominal bending-to-shear stress ratio was 0.5 to 1.7 for combined bending-torsion fatigue. Three different crack systems were found during testing: longitudinal cracks (L), transverse cracks (T), and cracks along the transverse welds (TW). Results were compared using the maximum principal stress and von Mises criteria. It was found that the maximum principal stress criterion was not relevant for proportional or non-proportional combined bending-torsion loading. It can be noted that Dahle et al. (1997) report both weld root and weld toe failures, but only the weld toe failures are here re-analysed.

3.2 Experimental program

3.2.1 Background

Fatigue tests shown in this chapter have previously been published by Bäckström et al. (1997a). They performed bending only, torsion only and proportional and non-proportional combined bending-torsion fatigue tests. Specimens were square hollow section tube-to-plate joints in the as-welded condition (Figure 14). The bending only fatigue tests were conducted using Ohta's (et al. 1994) recommendation that uses a different stress ratio for each stress range. In all other tests the stress ratio was -1 or 0. A total of 22 specimens was tested and fatigue lives ranged between $1 \cdot 10^4$ and $2 \cdot 10^6$ cycles. Fatigue cracks initiated at the weld toe during bending only and combined bending-torsion fatigue tests. For torsion only tests, fatigue cracks initiated and grew in the base material near a corner of the tube. The hot spot principal stress range was compared to an approach employing critical plane concepts as the fatigue damage parameter. Both parameters were thickness corrected. It was found that the critical plane model resulted in a better correlation of the data than did the principal stress range.

3.2.2 Materials and specimen fabrication

The test component was a square hollow section manufactured by Rautaruukki ($100 \cdot 100 \cdot 5$; Fe 52) which was welded to a square plate ($200 \cdot 200 \cdot 20$; RAEX Multisteel). In order to prevent the failure of the weld material at the weld root, a sufficiently large throat thickness of the weld was selected, which makes stresses in the weld material small compared with those in the base material. The square hollow section was welded to the plate using a single-bevel butt weld with the nominal throat thickness of 7.8 mm. The welding was done with the MIG method and using a welding wire of OK 12.51. All specimens were tested as-welded conditions. The test component is presented in Appendix C.

3.2.3 Test facility

The test equipment consisted of 2 hydraulic actuators (± 100 kN each) which were controlled by the MTS control system (Figure 13). The programming of constant amplitude load histories was done by FlexTest and T/RAC software.

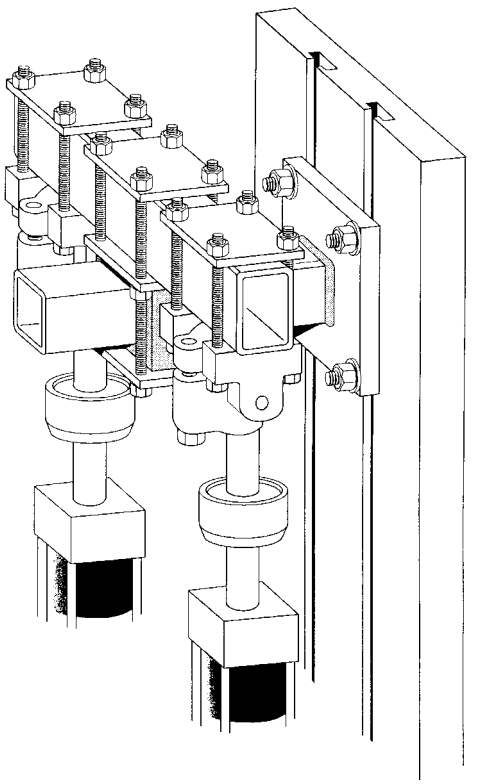

Figure 13. A schematic of the test equipment used in the fatigue tests.

The actuator forces were transferred to the component by a clamp that was attached at 249 mm from the plate surface (Figure 14). The cross-sectional distortion caused by the clamp was prevented by inserting a stiffener in the tube so the form of the cross-section could be preserved.

The measurement signals were recorded with the DASYLab PC application. In component calibration, the strain signals, actuator forces and strokes were meas-

ured and recorded. In the beginning of fatigue tests, the time histories of actuator forces and strokes were recorded.

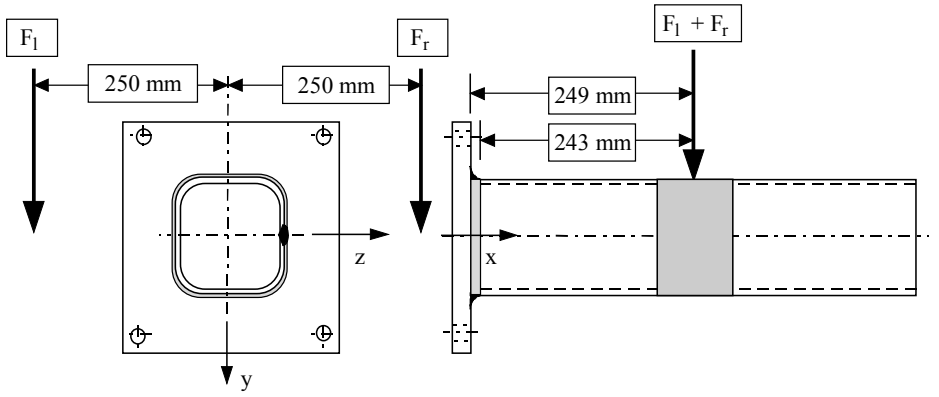

Figure 14. Bending and torsion lever arms and the co-ordinate system.

3.2.4 Component calibration

Eight rosette strain gauges of HBM1.5/350RY81 were attached to one component (Figure 15a), which was then used in the component calibrations. The rosette strain gauges were attached to the calibration component so that one grid ε_x was parallel to the longitudinal axis of the calibration component and two grids ε_{45} were at a 45° angle to the longitudinal axis of the calibration component. The distances of the hot spot rosette strain gauges from the weld toe were selected according to emeritus Professor Niemi's (1995) instructions (Figure 15b).

Strain ε_x was measured perpendicular to the weld at the upper flange of the calibration component close to the weld toe with six strain gauges (Figure 15). The strain ε_x was converted to structural stresses (σ_s) according to Hooke's relation, equation (31). A uniaxial stress state in the strain gauge location of the test component was assumed.

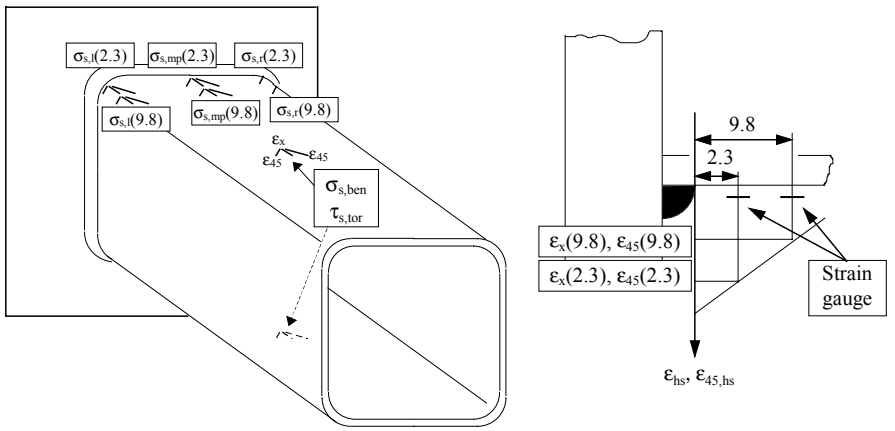

Figure 15. Rosette strain gauges: a) location in the calibrating component and b) distances from the weld toe.

$$\sigma_s = E\varepsilon_x \tag{31}$$

where $E = 2.1 \cdot 10^5$ MPa for steel.

The measured strain ε_{45} was converted to structural shear stress using generalized Hooke's law (Figure 15). By expressing the structural shearing stress (τ_s) by the measured strain ε_{45}, equation (32) was obtained.

$$\tau_s = \frac{E\varepsilon_{45}}{1+\nu} \tag{32}$$

where $\nu = 0{,}3$ for steel.

The nominal bending and torsional strains resulting from bending moment and torque, respectively, were measured at the mid-point between the end plate of the component and the clamp with two rosette strain gauges (Figure 15a). The rosette strain gauges were located at the upper and lower flange of the component. The measured strains were converted to structural stresses using Eq. (31) and (32).

The stresses in the square hollow section were calculated with elastic beam theory from measured actuator forces in bending only, torsion only and combined bending-torsion loading. The nominal normal stress (σ_{nom}) caused by the bending of the cantilever beam was calculated by using equation (33):

$$\sigma_{nom} = \frac{Fl}{W} \tag{33}$$

The nominal shearing stress (τ_{nom}) caused by the torsion of the cantilever beam was calculated with the elastic beam theory from equation (34):

$$\tau_{nom} = \frac{F_t l_t}{W_t} \tag{34}$$

A total of 9 static component calibrations were performed consisting of 3 sets of bending only, torsion only and combined bending-torsion loading. The SCFs for the bending and torsion loading cases are shown in Table 2. The (K_s) -values in are linear extrapolation results from the strain readings using two strain gages. If FE-methods are employed with a cubic extrapolation, a value of $K_{s.\sigma} = 3$ results (Lehtonen 1997).

Table 2. Measured structural stress concentration factors (SCF) under bending and torsion loading.

	Force $F = F_l + F_r$				Force $F_t = F_r - F_l$		
SCF in bending	10 [kN]	20 [kN]	30 [kN]	SCF in torsion	10 [kN]	20 [kN]	30 [kN]
$K_{s.\sigma,l}$	2.2	2.5	2.7	$K_{s.\tau,l}$	0.9	1.0	1.1
$K_{s.\sigma,mp}$	0.7	0.8	0.8	$K_{s.\tau,mp}$	0.8	0.9	1.0
$K_{s.\sigma,r}$	2.1	2.3	2.6	$K_{s.\tau,r}$	0.9	1.0	1.0

For torsion only loading, the strain gage instrumentation described in Figure 15 proved unsatisfactory (see Table 2) due to the highly localised torsion stress gradient. Again, using FEA with a cubic extrapolation, a value of $K_{s,\tau} = 1.3$ at weld toe (Lehtonen 1997).

3.2.5 Cracking observation

In bending fatigue tests cracks initiated from the outside corner of the RHS at the weld toe as anticipated (Figure 16a). The structural SCF (measured with strain gages and calculated using FEA) of a virgin specimen was greater in magnitude at that location than at the middle of the flange. The cracks growth was confined along the weld toe towards the middle of the flange.

Torsion only fatigue cracks initiated and *did not grow* at the weld toe (surface or root side), but within the base material of the tube (approx. 125 mm away from the weld toe). The critical location was the inside corner where the radius was the smallest (yet within the manufacturing tolerances) of the four corners (Figure 16b). Initial FEA results indicated that the torsion induced stresses of the RHS plate weldment were smaller at the weld root than those at the weld toe. More detailed FE-analysis were performed after the cracking observations (Lehtonen 1997). The results indicated that the magnitude of the torsion induced shear stresses were significantly larger in the fatigue crack initiation location (ie. at the tube base material, approx. 125 mm from the weld) than at the weld root.

Considering the proportional tests (Figure 17, paths D & E), 8 specimens failed from the outside corner of the RHS at the weld toe, as anticipated. Specimen no. 9 ($\sigma_{max} / \tau_{max} = 0.9$, path D) exhibited fatigue cracking similar to (Figure 16b). There is not enough experimental data to reflect whether the cracking behavior depends e.g. on the ($\sigma_{max} / \tau_{max}$) -ratio or the fatigue life regime (N_f). Due to the lack of published experimental data on similar welded joints subjected to similar loading conditions, comparisons are difficult. All non-proportional test specimens (Figure 17, path F) failed from the weld toe at the outside corner of the RHS.

a) b)

Figure 16. Observed cracks in a) bending and b) torsion test specimen.

3.2.6 Fatigue tests

Bending fatigue tests were conducted using Ohta's method (et al. 1994) from the nominal yield limit f_y = 355 MPa downwards (Figure 17, path A). Stress ratio R was different in each test. The nominal normal stress range ($\Delta\sigma_{nom}$) in the bending loading case was identical in magnitude and orientation to the nominal principal stress range ($\Delta\sigma_{1, nom}$). A total of 5 tests were conducted. The torsion fatigue tests were conducted with R_τ = -1 and R_τ = 0 (Figure 17, paths B & C). The nominal shear stress range ($\Delta\tau_{nom}$) was identical in magnitude to ($\Delta\sigma_{1, nom}$). Four tests were conducted.

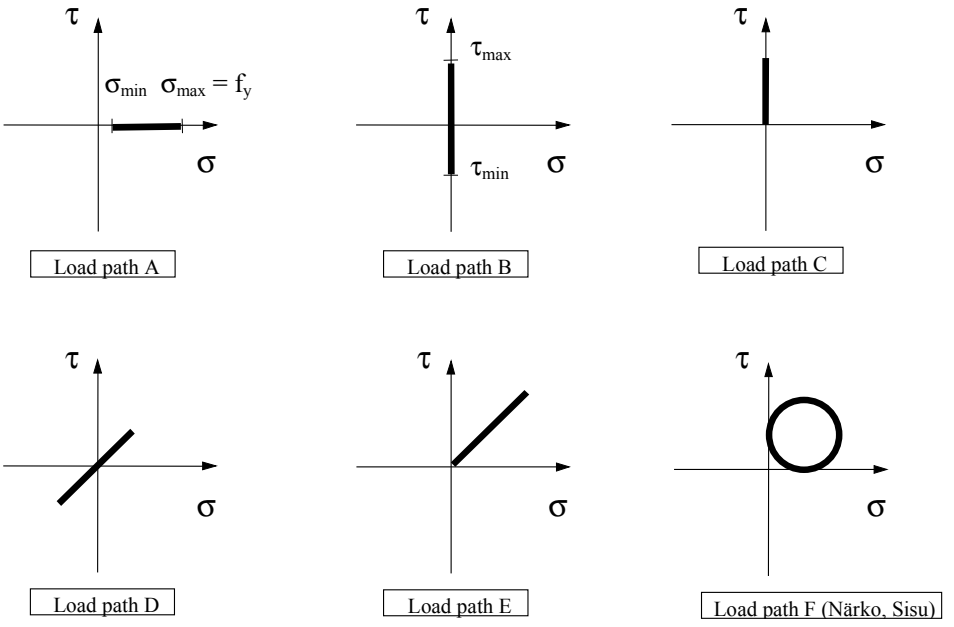

Figure 17. Loading paths employed in the fatigue tests. Normal stress σ (bending) as a function of shearing stress τ (torsion). Time axis towards the viewer.

The in-phase tests were conducted using $R = R_\tau = -1$ (Figure 17, path D) and $R = R_\tau = 0$ (Figure 17, path E). The nominal stresses were calculated from the measured actuator forces; calculation results were verified using strain gage measurement results. A total of 9 tests were conducted. The non-proportional fatigue tests were conducted using a constant phase shift (90°) between the normal and shearing stress. Stress ratio of $R = R_\tau = 0$ was employed (Figure 17, path F). The non-proportional multiaxial loading histories were gathered from typical duty-cycle events from field measurements for vehicles in the Finnish part of KONSPRO project (Bäckström et al. 1997b, Siljander et al. 1997a and 1997b). The nominal stresses were calculated and verified as above. A total of 4 tests were conducted. The fatigue test results are summarised in Table 3.

Table 3. Fatigue test results of the rectangular tube to plate joint.

Spec. [nr]	Load Path	R	R_τ	σ_{max}/τ_{max}	σ_{max} [MPa]	τ_{max} [MPa]	$\Delta\sigma$ [MPa]	$\Delta\tau$ [MPa]	$\Delta\sigma_{1,\,nom}$ [MPa]	N_f [cycles]
2	A	0.3	-	∞	355	0	266	0	266	45 000
1	A	0.1	-	∞	355	0	319	0	319	127 000
3	A	0.6	-	∞	355	0	149	0	149	274 000
5	A	0.7	-	∞	355	0	116	0	116	692 000
4	A	0.7	-	∞	357	0	98	0	98	1 110 000
7	B	-	-1	0	7	163	7	327	331	40 000
8	B	-	-1	0	6	134	7	270	274	160 000
6	B	-	-1	0	7	76	6	151	154	> 627 000
16	C	-	0	0	13	221	23	218	230	520 000
11	D	-1	-1	3.0	207	70	405	139	448	44 000
12	D	-1	-1	2.3	178	78	356	155	414	122 000
9	D	-1	-1	0.9	100	110	198	221	341	274 000
10	D	-0.8	-1.2	2.3	134	59	244	130	300	1 081 000
13	D	-0.8	-1.3	2.4	136	56	243	129	299	1 467 000
15	E	0	0	2.2	351	158	348	160	410	11 000
14	E	0	-0.1	1.8	237	131	227	140	294	95 000
17	E	0	0	2.3	255	113	254	116	299	120 000
18	E	0	0	2.2	211	96	208	99	248	345 000
19	F	0	0	2.3	255	111	253	111	221	100 000
22	F	0	0	2.3	257	111	254	111	221	148 000
20	F	0	0	2.3	211	91	207	92	183	413 000
21	F	0	0	2.3	211	92	208	93	183	529 000

3.3 Fatigue classes

3.3.1 Design

The success or failure of the interaction equation method is partially dependent on the ability to relate the welded structure of interest to one of the classified details in the design recommendation. Even for the relatively simple details evaluated here, see Figure 12, there is some disagreement in the codes about how the welded joint would behave under simple uniaxial loading. Fatigue class is defined as the stress range corresponding to $2 \cdot 10^6$ cycles to failure at a 97% survival probability. In most cases there is little difference between the design codes, but for some welds the fatigue class may differ by 50% or more. Nominal normal stress design fatigue classes for test specimens in Figure 12 and Figure 14 for the three codes are summarised in columns 4, 6 and 8 of Table 4.

Specimen in Figure 12a) was considered as a circular hollow section with intermediate plate (Figure 18b) for Eurocode 3 and IIW analysis. Fatigue classes varied slightly depending on the plate thickness. However, it would also be possible to alternately select a cruciform joint (Figure 18a) or circular hollow section welded to component classification (Figure 18c). For SFS 2378, specimens in Figure 12a) were analysed as cruciform joints because tube joint details are not given in that standard. Specimen in Figure 12b) was considered as a longitudinal attachment, which is common in every code, but different codes had different classification depending on the attachment length.

Some specimens in Figure 12a) and Figure 12c) were machined (Sonsino 1995, 1997), but this was not considered since Eurocode 3 and IIW do not provide for fatigue strength improvement due to machining. IIW has a provision that improved fatigue strength due to machining may be included if verification testing is performed. For machined tube-to-tube welds in SFS 2378, a ground butt weld detail classification was used. In stress relieved test specimens, the low internal residual stresses was taken into account by reducing the compressive part of the stress range according to rules given in different codes.

Table 4. Detail category for normal stress for different test specimen geometries according to SFS 2378 (1992), Eurocode 3 (1992) and IIW recommendations (Hobbacher 1996). The slope constant of the S-N curves is m = 3.

Test specimen	Figure 12	SFS 2378		Eurocode 3		IIW recommendations	
		Table 2	FAT	Table	FAT	Table {3.2}-1	FAT
Archer (1987)	b	No. 10a	71	9.8.4, No. 1	80	No. 521	71
Yung and Lawrence (1986)	a	No. 17	63	9.8.6, No. 6	50	No. 422	50
Siljander et al. (1992)	a	No. 17	63	9.8.6, No. 6	56	No. 422	56
Sonsino (1995, 1997) Tube-Tube	c	No. 3[1]	80	9.8.6, No. 3	71	No. 232	71
Sonsino (1995, 1997) Tube-to-plate	a	No. 16	71	9.8.6, No. 6	56	No. 422	56
Razmjoo (1996)	a	No. 17	63	9.8.6, No. 6	50	No.422	50
Bäckström et al. (1997a)	Figure 14	No. 16	71	9.8.6, No. 7	45	No. 424	45
Dahle et al. (1997)	d						
TW		No. 20	112	9.8.3, No. 5	90	No. 226[2]	112
T		No. 7	100	9.8.2, No. 6	100	No. 323	90

[1] Machined welds FAT 125 see Table 2 No.1.

[2] The weld of the test specimen was not ground flush.

Nominal shear stress design fatigue classes for test specimens in the Figure 12 and Figure 14 are summarised in columns 2, 3 and 4 of Table 5. For the shear stress SFS 2378 uses a SN slope of $m_\tau = 3$ while Eurocode 3 and IIW use a slope of $m_\tau = 5$.

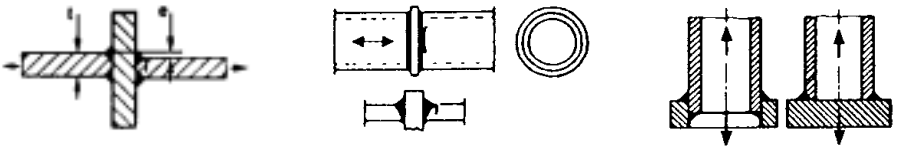

FAT 71 *FAT 56, T >8 mm* *FAT 50*

FAT 50, T ≤ 8 mm

a) *b)* *c)*

Figure 18. Potential fatigue classes for circular tube-to-plate joints according to IIW recommendations (Hobbacher 1996): a) cruciform joint (Table {3.2}-1, No. 412), b) splice of circular hollow section with intermediate plate (Table {3.2}-1, No. 422) and c) circular hollow section welded to component (Table {3.2}-1, No. 913).

Table 5. Detail category (FAT) for shear stress for different weld geometries according to SFS 2378 (1992), Eurocode 3 (1992) and IIW recommendations (Hobbacher 1996). The slope constants of the S-N curves are m_τ = 3 for SFS 2378 and m_τ = 5 for Eurocode 3 and IIW recommendations.

Test specimen	SFS 2378 Table 2, No. 28	Eurocode 3 Table 9.6.2	IIW recommendations Table.{3.2}-2
Archer (1987)	63	80	80
Yung and Lawrence (1986)	63	80	80
Siljander et al. (1992)	63	80	80
Sonsino (1995, 1997) Tube-Tube	63	100	100
Sonsino (1995, 1997) Tube-to-plate	63	100	100
Razmjoo (1996)	63	80	80
Bäckström et al. (1997a)	63	100	100
Dahle et al. (1997)			
TW	63	100	100
T	63	80	80

3.3.2 Mean

Fatigue strength of the different weld details can also be determined based on the bending/axial only fatigue data and the torsion only data. As an example, mean nominal normal stress S-N curves obtained from the stress relieved tubular specimens and for the stress relieved and machined tubular specimens are shown in Figure 19. Curves for all details were determined using simple linear regression anaysis with an assumed S-N slope of 3. Mean fatigue classes are defined as the stress range corresponding to $2 \cdot 10^6$ cycles to failure. These are summarised in columns 4, 6 and 8 of Table 6. Column 1 in this table gives the name assigned to the test series and the number of data points used in determination of the S-N curve is given in the second column. The first value gives the number of data points for normal stress and the second value is the number of points used to determine the shear curve.

In several cases the published references did not provide sufficient data to perform the regression analysis. Normal stress data was not published for Sonsino's tube-to-plate test specimens and only a few data points are given for Archer's and Dahle et al.'s test series. For stress relieved specimens IIW includes a procedure for eliminating a portion of the compressive load cycle in stress relieved structures. In non-stress relieved structures the entire load range is considered damaging while only a portion of the cycle is damaging for stress relieved specimens. This produces some differences between fatigue classes for nominal normal stress for the different analysis methods.

Nominal shear stress S-N curves obtained from the test data are shown in Figure 20a using slope of $m_\tau = 5$ as recommended by Eurocode 3 or IIW and in Figure 20b using an S-N slope of $m_\tau = 3$ as recommended in SFS 2378. Nominal shear stress fatigue classes for test specimens are summarised in columns 5, 7 and 9 of Table 6. It should be noted that no data was available to determinate the nominal shear stress S-N curves for three of test series reported by Sonsino or for the test series of Bäckström et al. and Dahle et al. In these cases the shear curve from one of the other data sets is used. The specimen that had geometry most closely resembling that for which the data is lacking was chosen. This is also indicated in Table 6.

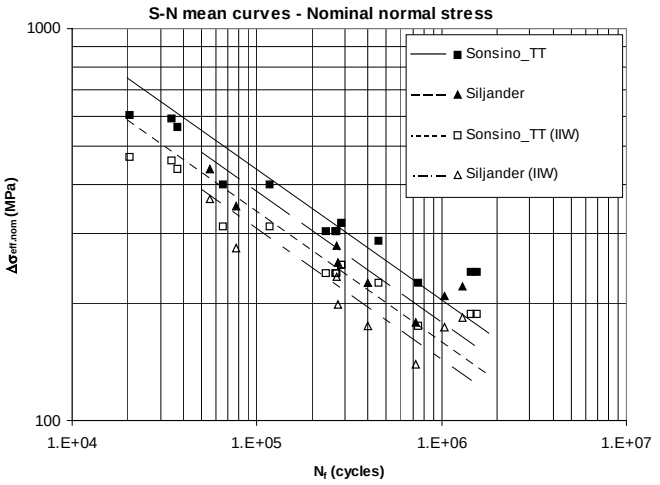

a)

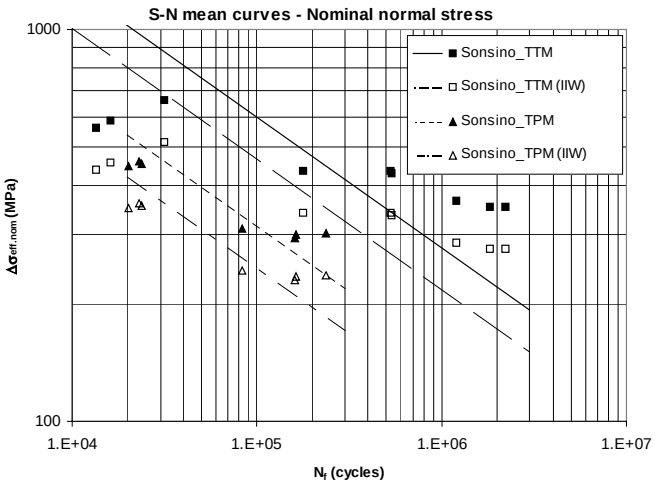

b)

Figure 19. S-N mean curves for nominal normal stress obtained from test data for the a) stress relieved test specimens and b) stress relieved and machined test specimens.

Table 6. Normal and shear stress mean fatigue classes for different test specimens obtained from test data using SFS 2378 (1992), Eurocode 3 (1992) and IIW (Hobbacher 1996).

Test series	Data points	Figure 12	SFS 2378		EC 3		IIW	
			$\Delta\sigma_C$	$\Delta\tau_C$	$\Delta\sigma_C$	$\Delta\tau_C$	$\Delta\sigma_C$	$\Delta\tau_C$
Archer (1987)	1/8	b	119	100	119	110	119	110
Yung and Lawrence (1986)	5/2	a	191	176	191	205	191	205
Siljander et al. (1992)	8/7	a	141	125	141	145	114	145
Sonsino (1995, 1997)								
tube-tube	14/-	c	161	131[1]	161	197[1]	126	197[1]
tube-tube mach.	9/6		220	131	220	197	172	197
tube-to-plate	-/-	a	116[2]	125[3]	116[2]	145[3]	90[2]	145[3]
tube-to-plate mach.	7/-		116	125[3]	116	145[3]	90	145[3]
Razmjoo (1996)	7/2	a	83	137	83	133	83	133
Bäckström et al. (1997a)	5/-	Figure 13	86	125[3]	86	145[3]	86	145[3]
Dahle et al. (1997)								
TW	3/-	d	103	100[4]	103	110[4]	103	110[4]
T	3/-	d	178	100[4]	178	110[4]	178	110[4]

[1] Tube-tube (mach.) data used in analysis
[2] Tube-to-plate (mach.) data used in analysis
[3] Siljander et al.'s data used in analysis
[4] Archer's data used in analysis

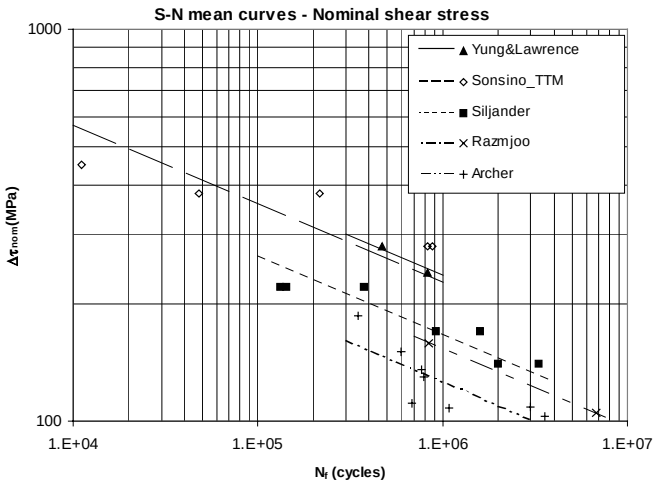

a)

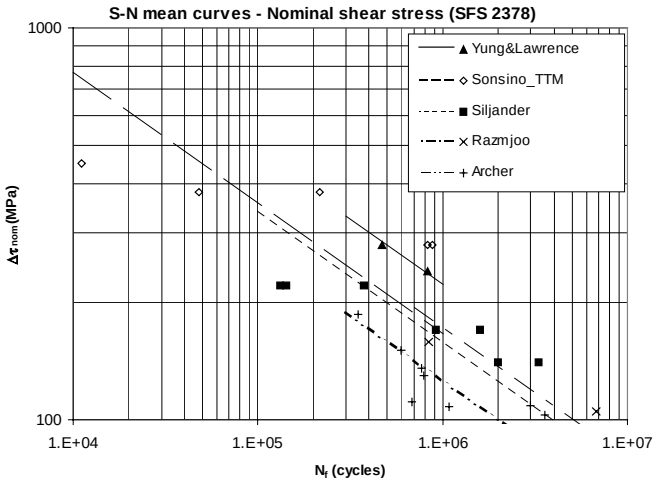

b)

Figure 20. S-N mean curves for nominal shear stress obtained from test data using S-N curve slope a) $m_\tau = 5$ and b) $m_\tau = 3$.

3.4 Structural stress concentration factors

Table 7 presents structural stress concentration factors for the five specimens shown in Figure 12 and Figure 14. Lehtonen (1997) has calculated the structural stress concentration factors for normal and shear stress for Siljander's version of specimen Figure 12a and for specimen Figure 14 using solid elements. Lehtonen has also determined the structural stress concentration factor for normal stress for Sonsino's version of specimen Figure 12a. The normal and shear stress concentration factors for the tube-to-tube specimen, Figure 12c, are expected to be small and are assumed to be unity in this study. Because of the nearly identical geometry, the specimens of Yung and Lawrence are considered to have the same structural stress concentration factors as those of Siljander. Structural stress concentration factors for Razmjoo's version of specimen Figure 12a are estimated from Lehtonen's FE-calculations employing slightly different boundary conditions.

The stress concentration factors of Siljander's test specimen were calculated using a non-rigid bolted boundary condition and Razmjoo's with fixed boundary conditions. For Archer's test specimen, Figure 12b, the structural stress concentration factor for normal stress was calculated with a parametric formula (Niemi et al. 1998). It is not clear if Archer's reported stress values are nominal or include some notch effect. Here it is assumed that the reported stresses are nominal, but if the reported values do include some notch effect, the hot spot stresses may be 10–20% too large. The structural stress concentration factor for shear stress was assumed to be unity in this study.

Table 7. Structural stress concentration factors.

Test specimen	Figure 12	Thickness mm]	$K_{s,\sigma}$	$K_{s,\tau}$	Type of weld
Archer (1987)	b	6.0	1.8	1.0	Fillet weld
Yung and Lawrence (1986)	a	8.0	1.25	1.1	Fillet weld
Siljander et al. (1992)	a	9.5	1.25	1.1	Fillet weld
Sonsino (1995, 1997) Tube-Tube	c	6.0	1.0	1.0	Butt weld
Sonsino (1995, 1997) Tube-to-plate	a	10	2.2	1.1	Full penetration fillet
Razmjoo (1996)	a	3.2	1.4	1.1	Fillet weld
Bäckström et al. (1997a)	Figure 14	5.0	3.0	1.3	Full penetration fillet
Dahle et al. (1997)	d	8 and 10	1.0	1.0	Butt and Fillet

4. Results

4.1 Re-analysis procedures

Figure 21 shows the flow chart of the re-analysis procedures used with interaction equations. The application of design and mean fatigue classes consist of three common steps. The common steps are: selection of the fatigue data for analysis, stress range reduction of the stress relieved specimens and choice of the interaction equations. The flow between design and mean fatigue class approaches differs from here on. Design fatigue classes are selected according to the rules of the codes and mean fatigue classes are determined directly from the test data. The re-analysis results are summarised in Figure 23 to Figure 28 where predicted life is shown versus experimental life. Some aspects of the interaction equations has been presented in the *Sixth International Conference on Biaxial/Multiaxial Fatigue & Fracture* (Bäckström & Marquis 2001a).

As Figure 22 shows, the re-analysis procedures applied to damage parameters starts with two common steps: selection of the fatigue data for analysis and the hot spot stress determination from the nominal stresses. The hot spot stresses are determined by multiplying the nominal normal and shear stresses obtained from the literature review and fatigue tests with structural stress concentration factors.

Principal stress range, maximum shear stress range, and a modified critical plane model for welds are used in the re-analysis as the damage parameters. Maximum principal stress range is determined from the maximum changes in the stress components during the loading event (Maddox 1991), maximum shear stress range is determined as the greatest algebraic difference between principal stresses during the whole loading event (ASME 1989) when the maximum hot spot effective shear range is determined using the critical plane approach described earlier. The relation between damage parameters and the experimental fatigue life are presented in Figure 29 to Figure 34. The re-analysis results for the damage parameters has been published in Fatigue & Fracture of Engineering Materials & Structures journal by Bäckström & Marquis (2001b).

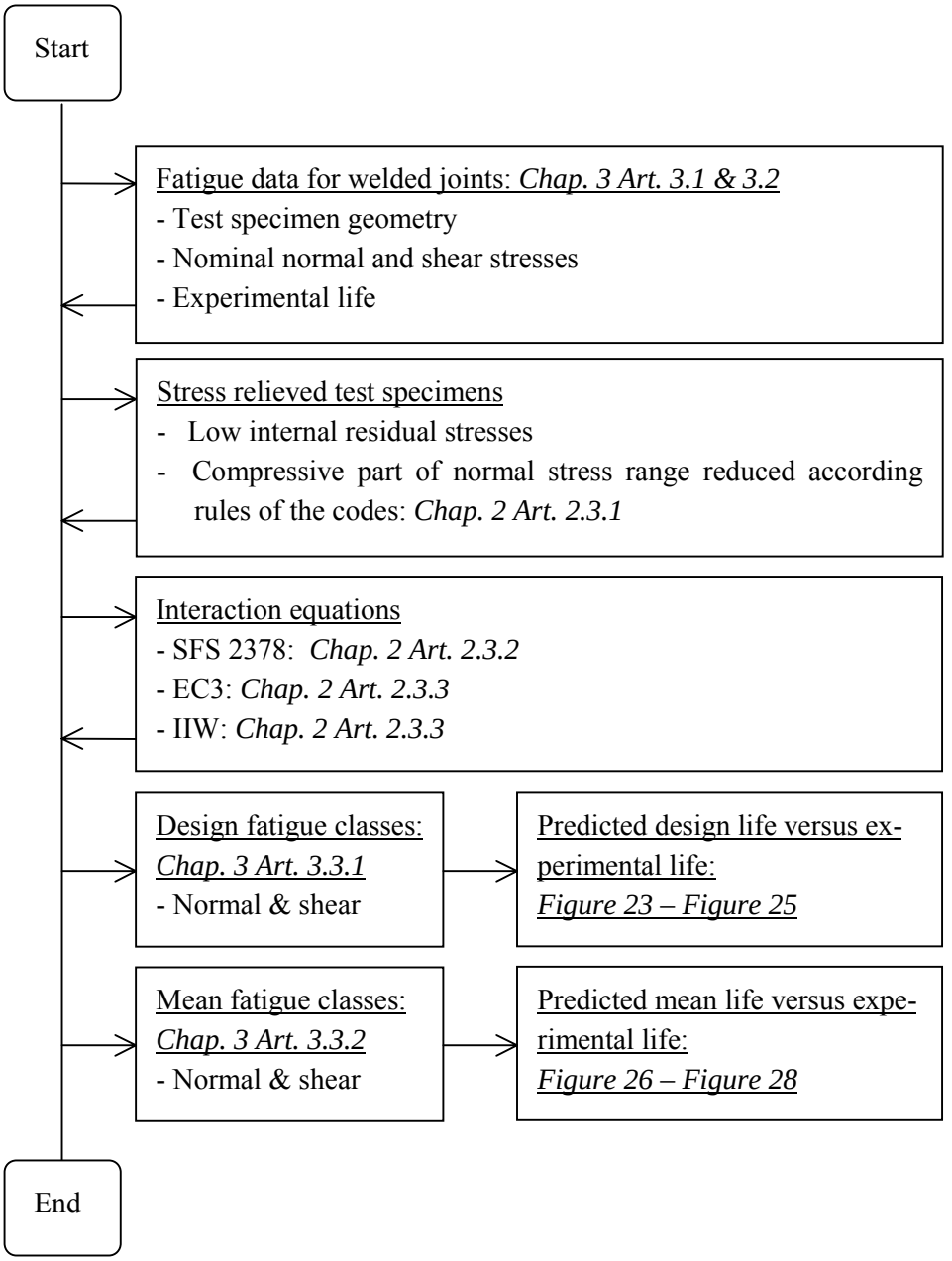

Figure 21. Re-analysis procedures used with interaction equations.

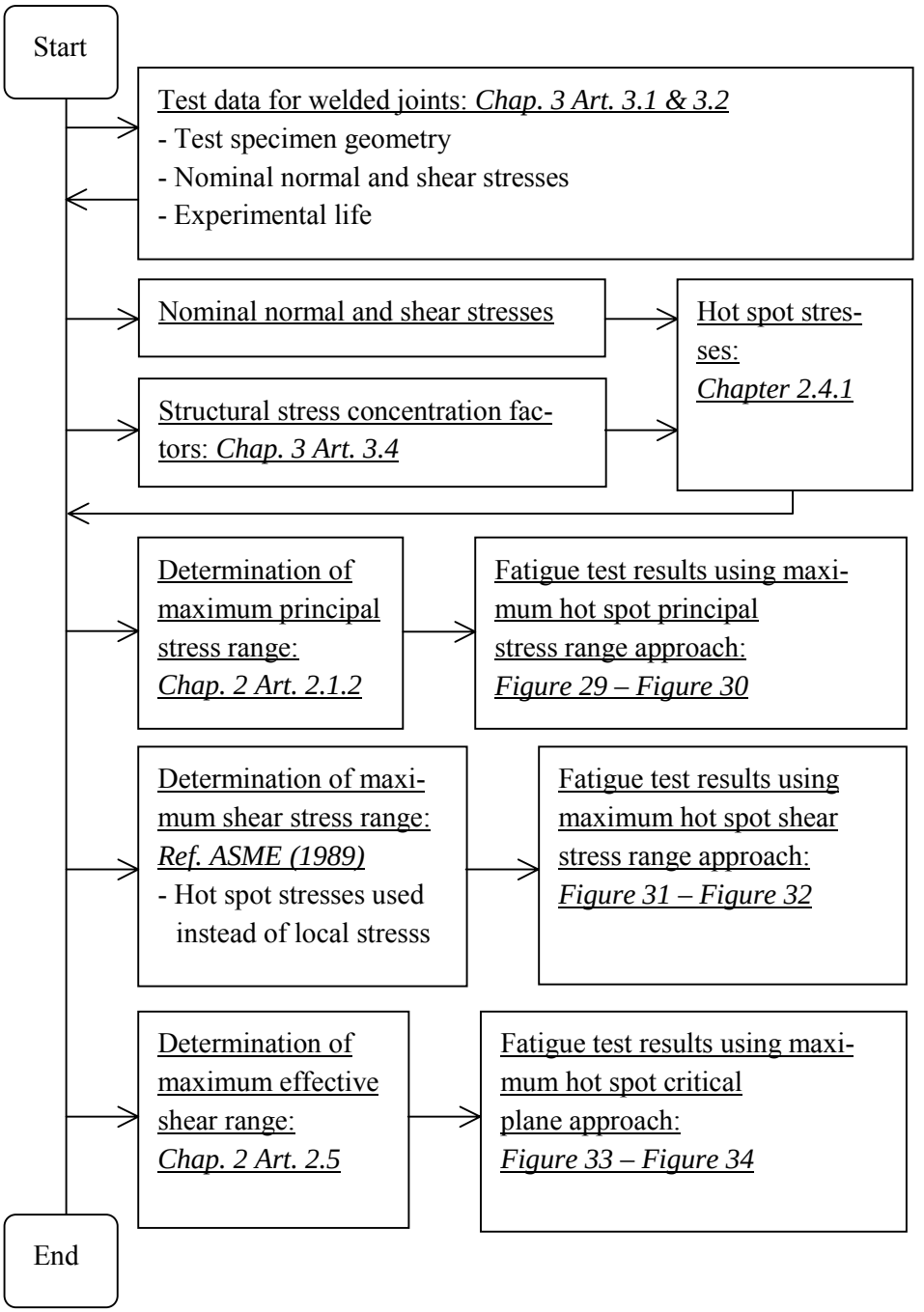

Figure 22. Re-analysis procedures used with damage parameters.

4.2 Nominal stress approaches

4.2.1 Interaction equations

Figure 23 shows the relationship between the predicted design fatigue life with interaction equations according to SFS 2378 using fatigue classes from Table 4 and Table 5 and experimental fatigue life obtained from testing. It should be noted that design life calculation necessarily contains a degree of conservatism which usually represents 3 % failure probability. This figure shows that design fatigue classes used with this interaction equation generally give conservative results, but the scatter was significant. The results obtained with interaction equations from Eurocode 3 or IIW are shown in Figure 24 and Figure 25. The scatter seems to be slightly greater than for SFS 2378 in Figure 23.

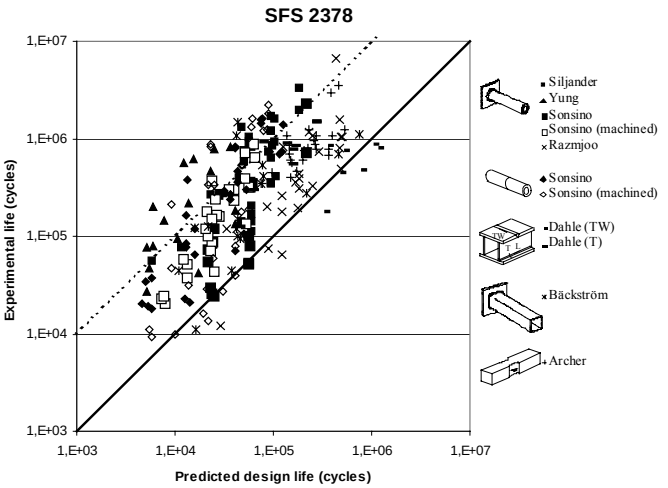

Figure 23. Fatigue test results for welded joints under multiaxial loading using nominal stresses and interaction equation from SFS 2378 (1992).

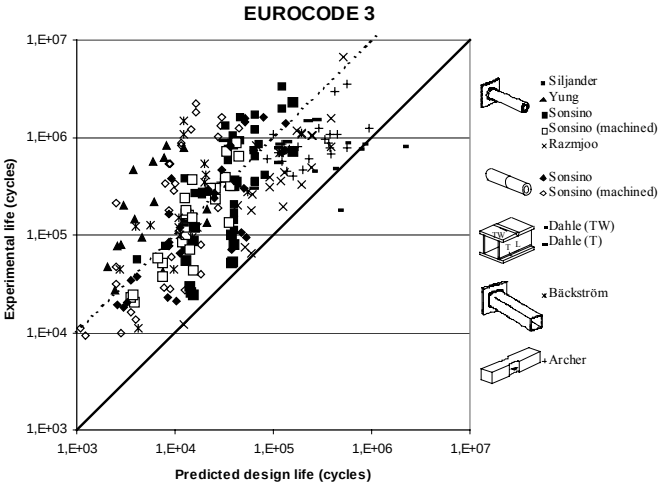

Figure 24. Fatigue test results for welded joints under multiaxial loading using nominal stresses and interaction equation from Eurocode 3 (1992).

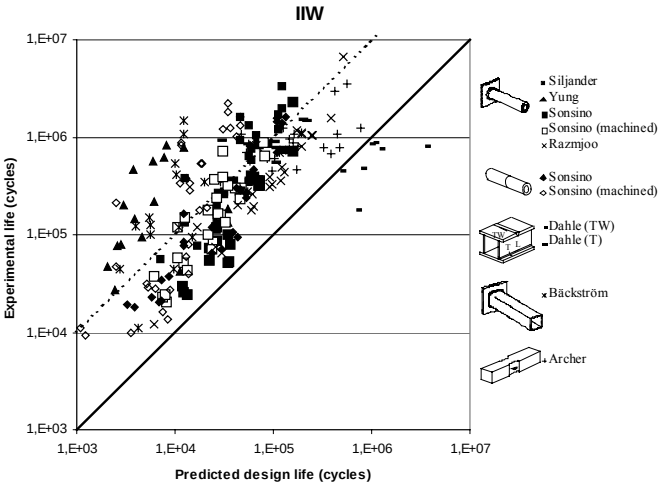

Figure 25. Fatigue test results for welded joints under multiaxial loading using nominal stresses and interaction equation from IIW recommendations (Hobbacher 1996).

Figure 26 to Figure 28 shows the relationship between the predicted fatigue life using interaction equations and mean S-N curves obtained from bending only and torsion only fatigue tests (Table 6) and experimental fatigue life obtained from testing. The fatigue life predictions were conducted according to SFS 2378 in Figure 26, Eurocode 3 in Figure 27 and IIW recommendations in Figure 28.

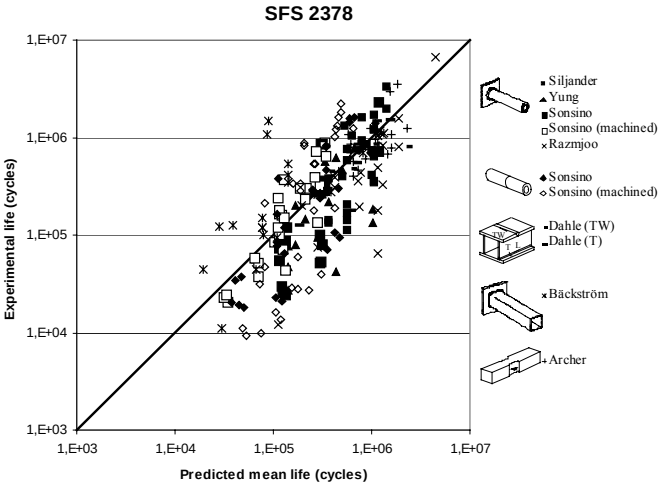

Figure 26. Fatigue test results for welded joints under multiaxial loading using nominal stresses and mean S-N curves with interaction equation from SFS 2378 (1992).

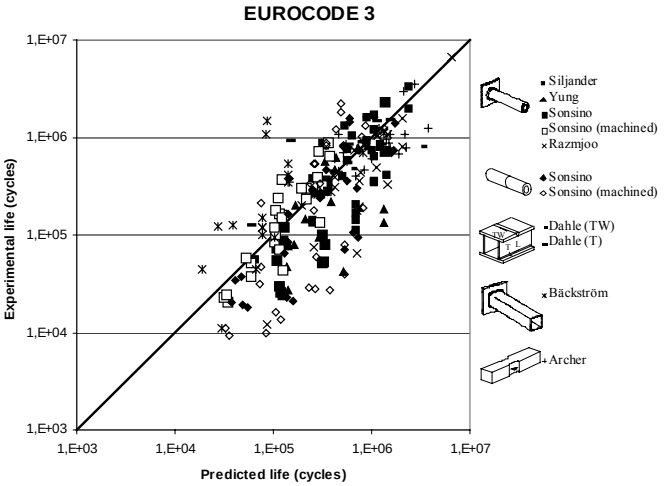

Figure 27. Fatigue test results for welded joints under multiaxial loading using nominal stresses and mean S-N curves with interaction equation from Eurocode 3 (1992).

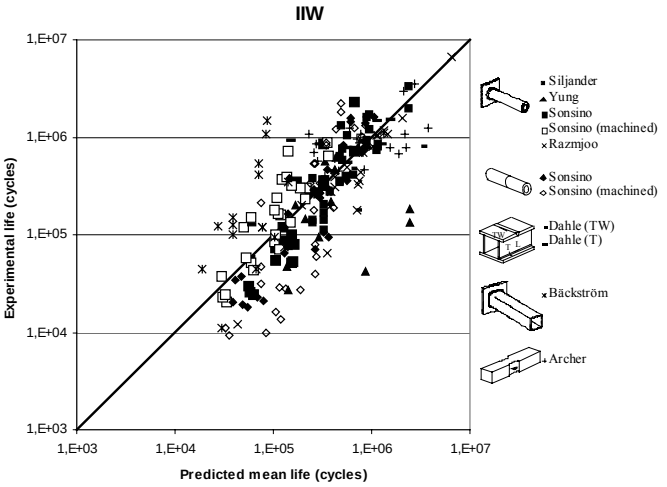

Figure 28. Fatigue test results for welded joints under multiaxial loading using nominal stresses and mean S-N curves with interaction equation from IIW recommendations (Hobbacher 1996).

4.2.2 Analysis of standard error

Standard error between the predicted mean fatigue life and experimental life for the three interaction equations was analysed by using Eq. (35). The standard error (sN) was sN_{SFS} = 0.399 for SFS 2378, sN_{EC3} = 0.416 for Eurocode 3 and sN_{IIW} = 0.380 for IIW. These differences are relatively small with the standard error for Eurocode 3 method being only about 9% greater than for the IIW method and the SFS2378 method being only 3% greater than for the IIW method. The main difference between IIW recommendations and Eurocode 3 was the damage summation for nonproportional loading. The interaction equation from SFS 2378 standard seems to be as good as IIW's equation even without the damage summation correction of 0.5 for nonproportional loading.

$$sN = \sqrt{\frac{\sum_{i=1}^{n}\left(\log\left(N_{i,predicted}\right)-\log\left(N_{i,experimental}\right)\right)}{n-1}} \tag{35}$$

4.3 Hot spot stress approaches

4.3.1 Maximum principal stress approach

In Eurocode 3 (1992) the application of maximum principal stress range for welded structures is recommended when the combined effect of bending and shear must be considered. Figure 29 shows the relationship between fatigue life of welded joints and maximum hot spot principal stress range. A total of 233 test results (Table 1) with weld toe failure under bending, torsion and proportional and non-proportional combined bending-torsion loading were obtained.

It should be noted that the assessment of maximum principal stress range is limited only to proportional loading cases in the design code. However, non-proportional fatigue test results are here included in the analysis. Maximum principal stress range is determined from the maximum changes in the stress components during the loading event (Maddox 1991). This means that the prin-

cipal stress range is determined at each point in time during the cycle from the changes in stress component, see chapter 2.1.2. For comparison of the effect of proportional and non-proportional loading, Sonsino's and Siljander's fatigue tests results are shown in Figure 30.

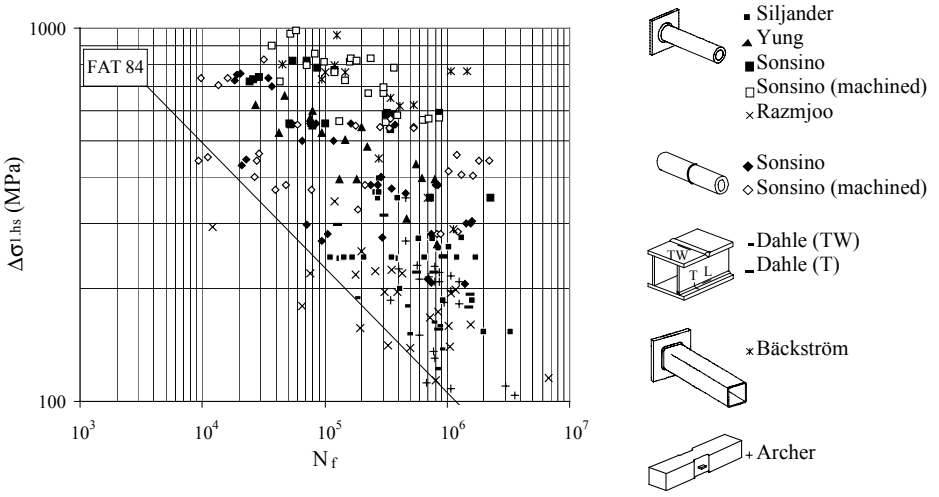

Figure 29. Fatigue test results for welded joints under multiaxial loading using the maximum hot spot principal stress range.

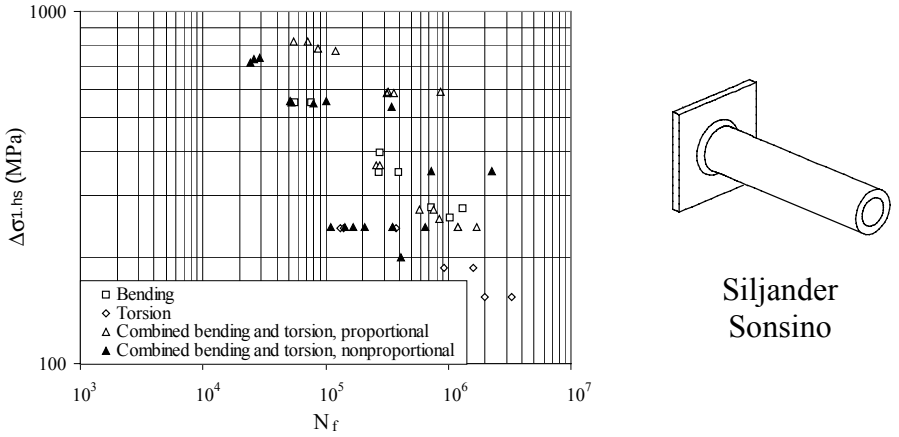

Figure 30. Fatigue test results for tube-to-plate welded joints under proportional (bending, torsion and combined bending and torsion) and non-proportional (combined bending and torsion) loading using the maximum hot spot principal stress range approach.

4.3.2 Maximum shear stress range

Maximum shear stress range is used as the damage parameter by ASME (1989) when the direction of the principal stresses change during the stress cycle. Maximum shear stress range is determined as the greatest algebraic difference between principal stresses during the whole loading event. Principal stresses are determined at each point in time during the cycle from the changes in the individual normal and shear stress components. This method may be used for welded structures if the principal planes are less than 45° apart, but may be too conservative for greater angles (Maddox 1991). It should be noted that the ASME code method is not here applied directly since it requires knowledge of the local stresses while this paper uses hot spot stresses. Test data for all specimens is plotted in terms of maximum hot spot shear stress range in Figure 31 and a smaller set of tube-to-plate specimen data is shown in Figure 32.

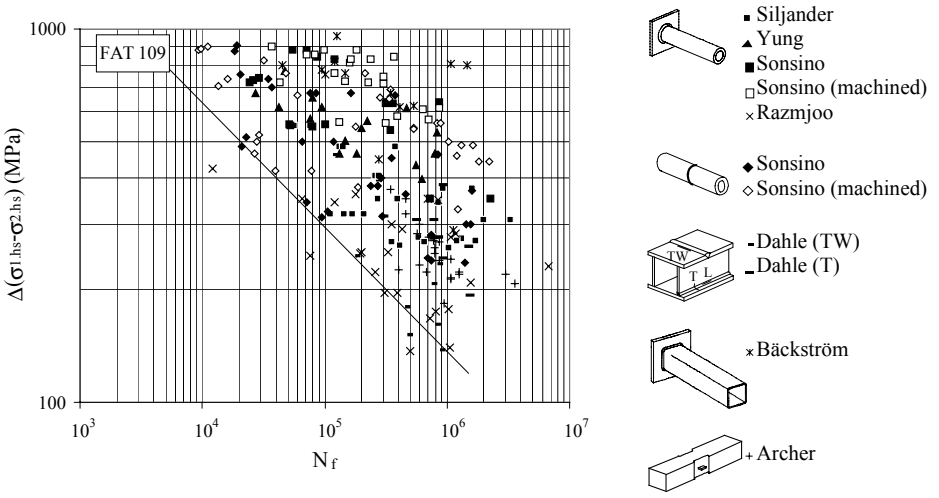

Figure 31. Fatigue test results for welded joints under multiaxial loading using the maximum hot spot shear stress range approach.

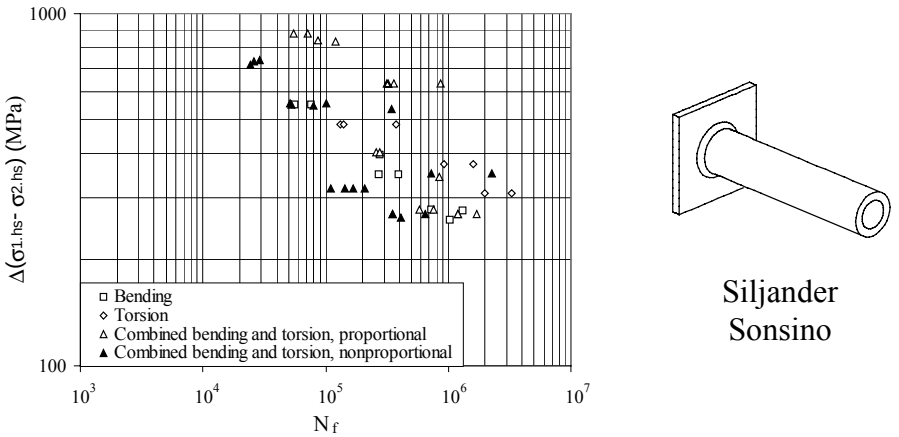

Figure 32. Fatigue test results for tube-to-plate welded joints under proportional (bending, torsion and combined bending and torsion) and non-proportional (combined bending and torsion) loading using the maximum hot spot shear stress range approach.

4.3.3 Modified critical plane model for welds

Test data for welded joints was also analysed using the critical plane approach described earlier. In the calculations, Findley's material constant k was assumed to be 0.3, which is a typical value for structural steel (Findley 1959). Figure 33 shows the relationship between fatigue life of welded joints and maximum hot spot effective shear range. The effect of proportional and non-proportional loading is illustrated by the smaller data set shown in Figure 34.

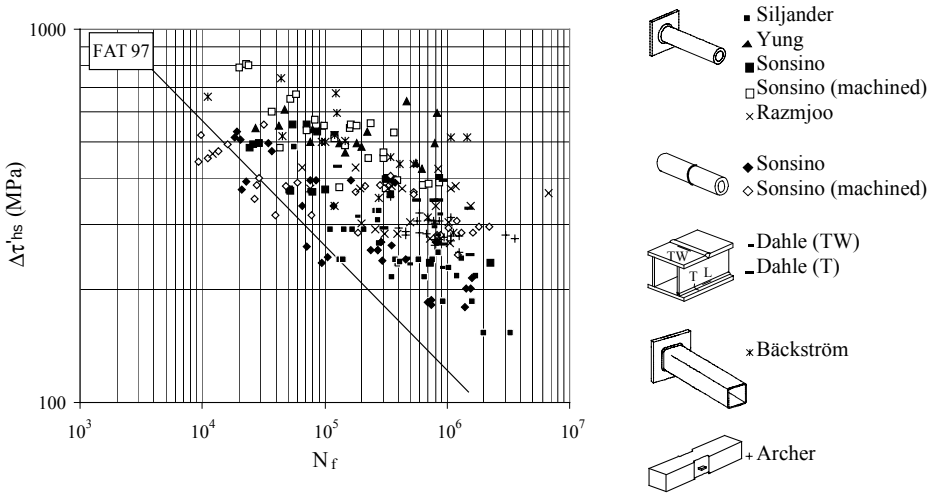

Figure 33. Fatigue test results for welded joints under multiaxial loading using the hot spot critical plane approach.

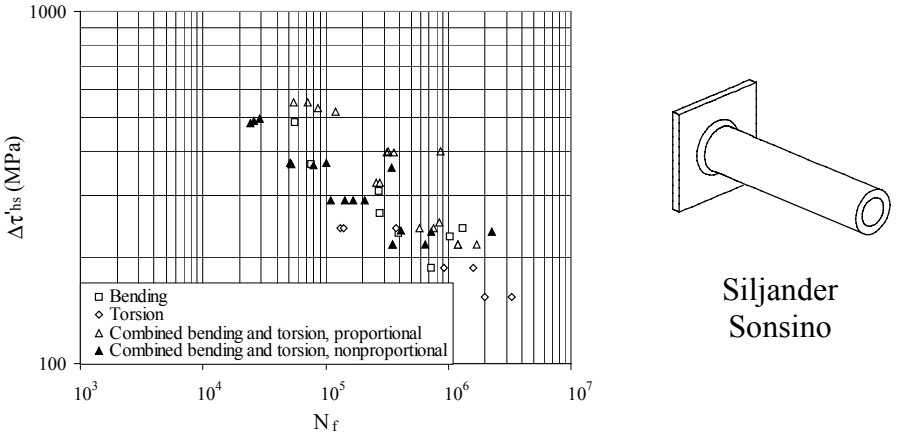

Figure 34. Fatigue test results for tube-to-plate welded joints under proportional (bending, torsion and combined bending and torsion) and nonproportional (combined bending and torsion) loading using the hot spot critical plane approach.

4.3.4 Evaluation of scatter

Scatter in Figure 29 – Figure 34 was analysed using linear regression by assuming S-N slopes of both 3 and 5 according to the method proposed by IIW recommendations (Hobbacher 1996). Table 8 summarises the analyses and shows the standard deviation in log(C), *s*, for each of the three analysis methods and two slopes. The upper part of the table shows all 233 data points representing weld toe failures while the lower part shows only the 49 circular tube-to-plate joints. As can be seen, the best correlation was obtained by using the critical plane approach. The hot spot shear stress range approach was better than the maximum principal stress range approach. The best fit design curve for all 233 data points was FAT 84 for maximum hot spot principal stress range (Figure 29), FAT 109 for maximum hot spot shear stress range (Figure 31) and FAT 97 for hot spot critical plane model (Figure 33) with a slope of 3.

Table 8. Analysis of data scatter for different methods.

Test series	Approach	*s* based on slope 3	*s* based on slope 5
All test data	$\Delta\sigma_{1.hs}$	0.61	1.02
(233 specimens)	$\Delta(\sigma_{1.hs} - \sigma_{2.hs})$	0.54	0.86
	$\Delta\tau'_{hs}$	0.47	0.58
Sonsino & Siljander	$\Delta\sigma_{1.hs}$	0.46	0.78
(49 specimens)	$\Delta(\sigma_{1.hs} - \sigma_{2.hs})$	0.41	0.60
	$\Delta\tau'_{hs}$	0.33	0.45

4.4 Application – Window corners from a passenger ferry

All details of the testing and the analysis of the window corners can be found from Fatigue 2000 conference paper (Bäckström et al. 2000). This chapter gives a short overview of the Fatigue 2000 paper as an example why the multiaxial fatigue of welded joints is an important issue.

Application of the Structural design of passenger ships is governed by the desire for light structures with flexible space usage thus maximising payload capacity and passenger comfort. In the past fatigue has not been a main design driver, but this has been gradually changing as the accuracy of stress analysis increases and structures are exploited closer to their fatigue limits. Modern ship design comprises ever-larger windows and open spaces leaving less structure to carry the loads. The use of higher yield strength steels potentially raises the overall stress level whereas the fatigue strength of welded joints remains largely unchanged.

Development of fatigue assessment procedures for promoting the use of higher tensile strength steels in ship design is being addressed by a European Union funded research project, FatHTS. One task of this project involves study of the fatigue strength of several typical structural details of various ship types. For passenger ships a window corner detail was chosen. This detail also represents other large openings in side shells and bulkheads.

Side shells of a passenger ship are loaded by shear forces associated with the global wave bending moment, Figure 35. Windows are typically arranged in rows on each of several decks. Shear forces are transmitted through the vertical strips between windows and the stress levels are defined by the deck stiffness, size of the windows and height and width of the strips. Clearly the critical design detail exists at the window corner area. The stress level at this detail tends to increase as the number of continuous longitudinal structures decreases and as windows become larger and more closely spaced. Detail design of the corner area has become increasingly important. It is necessary to check both the maximum stresses as well as the fatigue strength of this detail.

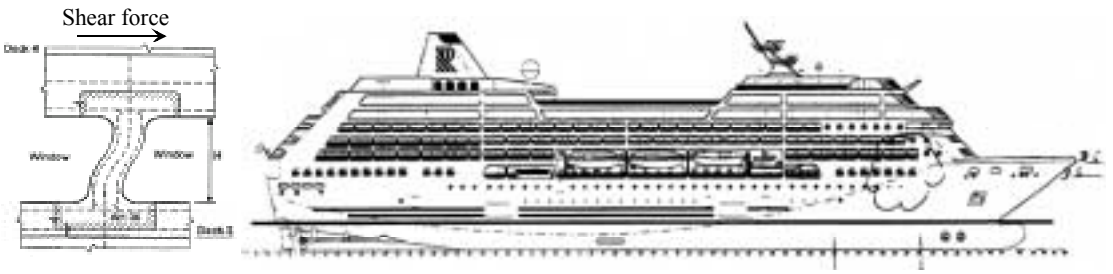

Figure 35. An example of a passenger ship by Chantier d'l Atlantique. A sketch is shown of the loading and deformation pattern at window area of the side shell.

Within the FatHTS project three alternative designs for the window corner detail were chosen for further testing and analysis. Large-scale specimens for fatigue testing were fabricated by Chantier d'l Atlantique in France and fatigue tests were conducted at VTT Manufacturing Technology, Finland. Figure 36 shows the T-shaped specimens which consisted of a vertical support column fixed to the floor and a horizontal beam loaded at both ends. A total of four specimens were fabricated by using thermomechanically processed DH 36 steel. The test matrix included constant amplitude fatigue tests for the three alternative designs. For one design variant a spectrum load fatigue test was performed by using a simulated wave load spectrum. Each specimen contained four geometrically similar fatigue critical details.

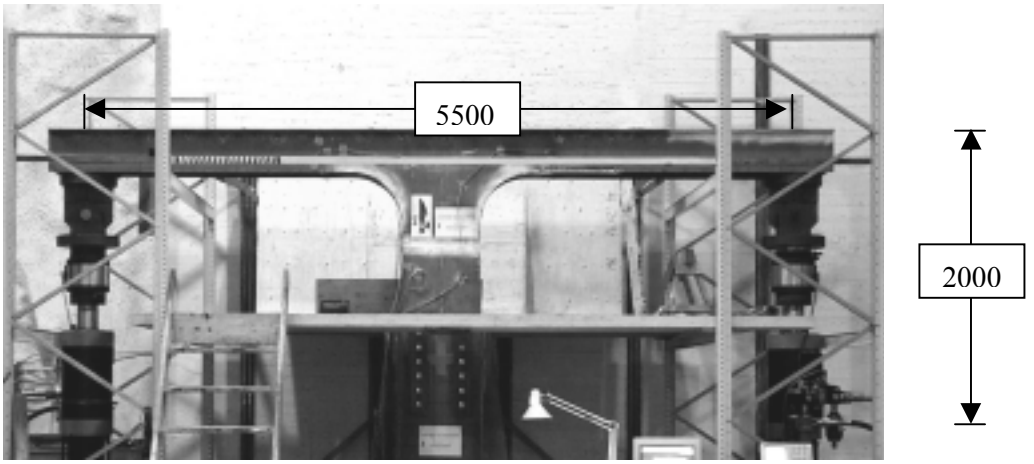

Figure 36. Test specimen and load rig (dimensions in mm).

A typical crack for test specimens with collar plates is shown in Figure 37a. The cracks initiated along the weld and propagated perpendicular to the maximum principal stress. The test results showed for the window corner design with a collar plate, that the principal stress correlated best with the fatigue life.

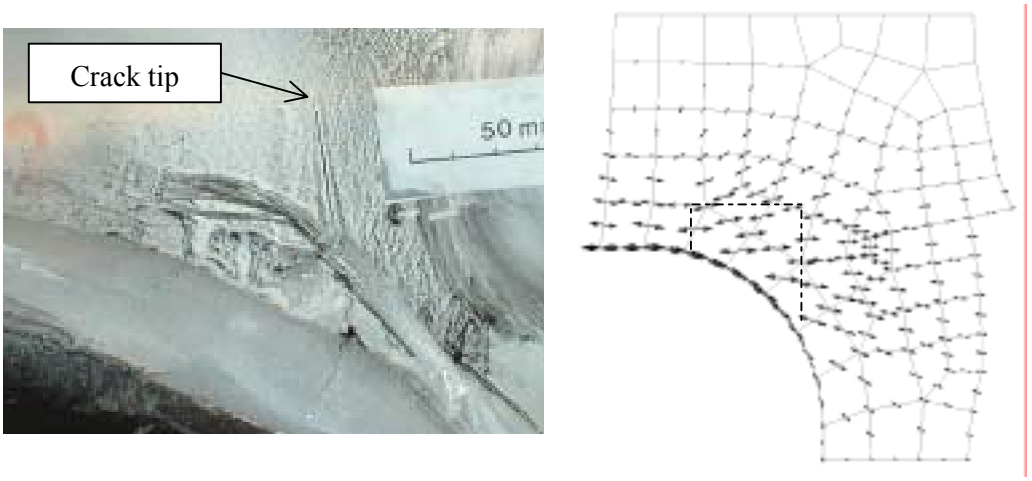

a) *b)*

Figure 37. a) Cracked specimen and b) direction and relative magnitude of maximum principal stresses according to FE-calculations.

5. Discussion

5.1 General

Design codes such as those presented in SFS 2378 (1992), Eurocode 3 (1992), or IIW recommendations (Hobbacher 1996) can greatly reduce the analysis effort in the design of welded structures. The use of design codes is also often required as part of the contractual process between designer and end user. Welded structures can be very complex and accurate structural analysis for fatigue life assessment is often the slowest aspect of the design process. Design codes seek to find a suitable balance point between computational accuracy and ease of use. Multiple loading points or eccentric loading will generally lead to multiaxial stresses that complicate the analysis process, especially when loads act in a non-proportional manner. Vehicle frames, pipelines, boom structures and window corners (see chapter 4.4) are only a few examples of welded structures that are subjected to multiaxial loads during service.

Design codes offer one or more methods for computing the critical stress in a structure for fatigue, e.g., nominal stress, structural stress, or local stress. These stress values are then related to fatigue strength via one or more S-N curves. In the case or multiaxial stresses, the codes recommend that S-N curves for normal stress and shear stress be combined with the aid of interaction equations. One advantage of using interaction equations as compared to, e.g., maximum principal stress range or critical plane type of approach, is the simplicity of the calculation of stress ranges. Computation of stress ranges and damage parameters in the case of nonproportional multiaxial loading may be very complicated. Even cycle counting, which has been standardised for uniaxial loading, is still the subject of some controversy for multiaxial fatigue (Socie & Marquis 2000).

It has been reported that nominal stresses do not correlate fatigue strength for multiaxially loaded welds as well as local stress approaches (Siljander et al. 1992, Sonsino 1997). Nominal stress ranges were reported for all fatigue tests which were found in the literature survey but weld geometry, e.g. reinforcement angle and toe radius, were not reported in all cases. Parametric formulae for hot spot stress (Niemi et al. 1998) and local stress (Iida & Uemura 1996) concentration factors for welded joints can be found in the literature but local stress concentra-

tion factors require knowledge of the local weld geometry making the nominal and hot spot stress approaches the only means for comparison. Also, during design, hot spot values do not require as detailed a stress analysis and are therefore more easily applied during the engineering stage of a structure. This is reflected in the newest recommendations for welded joints (Eurocode 3 1992, IIW recommendations by Hobbacher 1996) which now allow the use of the hot spot stresses. The hot spot stress approach has been shown to be an effective tool in the case of uniaxial loading and is worth considering also for multiaxial loading.

5.2 Interaction equations

Figure 23 shows the relationship between the predicted design fatigue life according to SFS 2378 using fatigue classes from Table 4 and Table 5 and experimental fatigue life obtained from testing. It should be noted that design life calculation necessarily contains a degree of conservatism which usually represents 3 % failure probability. This figure shows that design fatigue classes used with this interaction equation generally give conservative results, but the scatter was significant. The scatter was slightly greater for interaction equations from Eurocode 3 (Figure 24) and IIW (Figure 25). Of the three interaction equations previously described, SFS 2378 was the most successful in resolving the data to a single line according to the statistical methods. For some test specimens the experimental results consistently exceeded the design life, e.g., ▲Yung, while for other specimens the design fatigue life was often less than that obtained in the fatigue tests, e.g., ━ Dahle and x Razmjoo. Accuracy of the prediction is clearly related to the detail category selected, however, the differences between fatigue classes in different standards were small in most cases. Before these methods can be used for optimisation of structures, more work is needed to improve the generally over-conservative estimates.

Figure 26 to Figure 28 shows the relationship between the predicted fatigue life using interaction equations and mean S-N curves obtained from bending only and torsion only fatigue tests (Table 6) and experimental fatigue life obtained from testing. The fatigue life predictions were conducted according to SFS 2378 in Figure 26 and IIW recommendations in Figure 28. In both figures the data for machined specimens tends to be non-conservative at higher stress levels and moves to being conservative as the stress level decreases and fatigue life in-

creases. This observation is clearly the result of S-N curve slope, which is forced to be 3 for the analysis, but is in reality very different for the normal stress only load case. The interaction equations tend to give overly conservative prediction on data from Bäckström et al. It can be noted that both Bäckström et al. and Dahle et al. reported significantly different crack modes for the bending only or torsion only cases. For Bäckström et al. the cracking was in different locations, while for Dahle et al. the two load cases produced cracking in the same weld but torsion always produced root side cracking and bending often produced toe side cracking. For comparison the round tube-to-plate welds always produced circumferential cracks at the weld toe.

Bäckström et al. (1997a) has noted that the rectangular tube-to-plate connection has a high normal stress concentration that greatly influences fatigue life. Also, for the combined bending torsion load cases there is a systematic different in the data based on the applied stress ratio. Experiments done and R=-1 had significantly more fatigue strength than specimens loaded at R=0 even when the normal to shear stress ratio was nearly constant. This may indicate that some portion of the compressive load cycle was non-damaging for these specimens and that they should perhaps be treated more as stress relieved.

As seen from Figure 28, the interaction equations tended to give non-conservative predictions on some combined loading data from Yung and Lawrence. It is interesting to note that both under bending only and torsion only loading this series of specimens had fatigue strength much higher than would normally be expected based on the specimen geometry alone. This tends to produce overly optimistic life predictions for the combined loading cases. By contrast the same data tended to be overly conservative (Figure 25) when fatigue strength classes from the design codes were used.

In order to compare the effect of proportional and non-proportional loading, 31 proportional and 18 non-proportional test results for the circular tube-to-plate specimen shown in Figure 12a are considered. Data was obtained from three references (Siljander et al. 1992, Sonsino 1995 & 1997). Effects of combined loading are shown in Figure 38, Figure 39 and Figure 40 using design fatigue classes and in Figure 41, Figure 42 and Figure 43 using mean fatigue classes with interaction equations from SFS 2378, Eurocode 3 and IIW. Good correlation between proportional and non-proportional test results was obtained espe-

cially for the IIW interaction equation, which uses a damage summation of 0.5 for nonproportional loading. The increased damage of non-proportional loading in ductile materials has been attributed to fatigue damage being accumulated on numerous planes within the material (Sonsino & Maddox 2001).

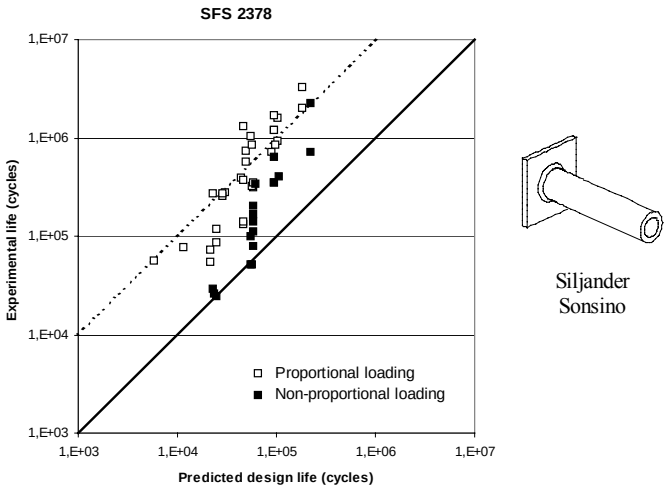

Figure 38. Re-evaluation of tube-to-plate welded joints under proportional and non-proportional loading using design fatigue classes with interaction equation from SFS 2378 (1992).

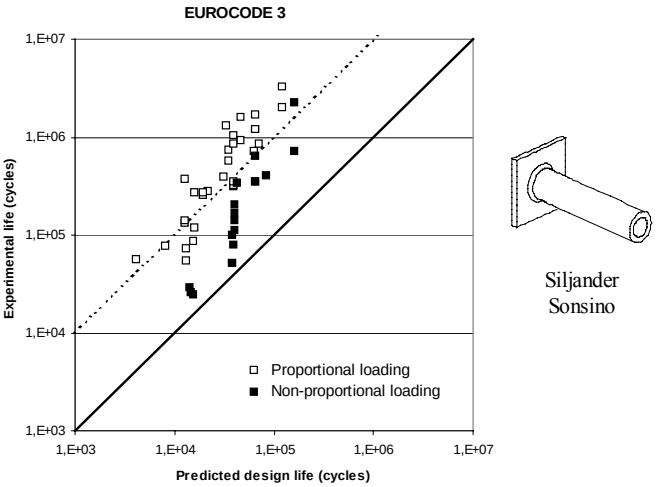

Figure 39. Re-evaluation of tube-to-plate welded joints under proportional and non-proportional loading using design fatigue classes with interaction equation from Eurocode 3 (1992).

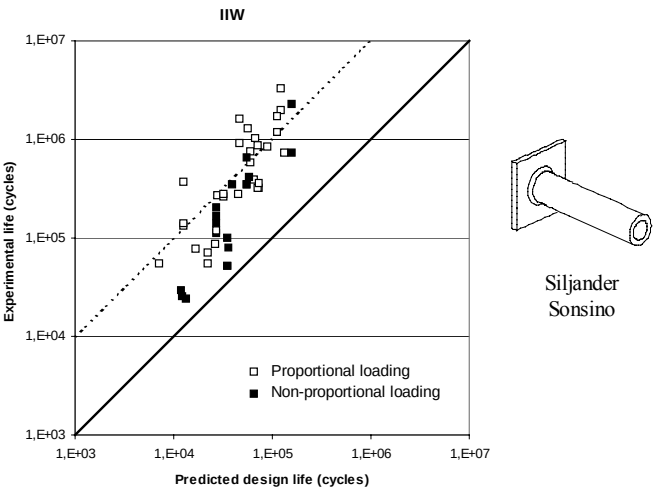

Figure 40. Re-evaluation of tube-to-plate welded joints under proportional and non-proportional loading using design fatigue classes with interaction equation from IIW recommendations (Hobbacher 1996).

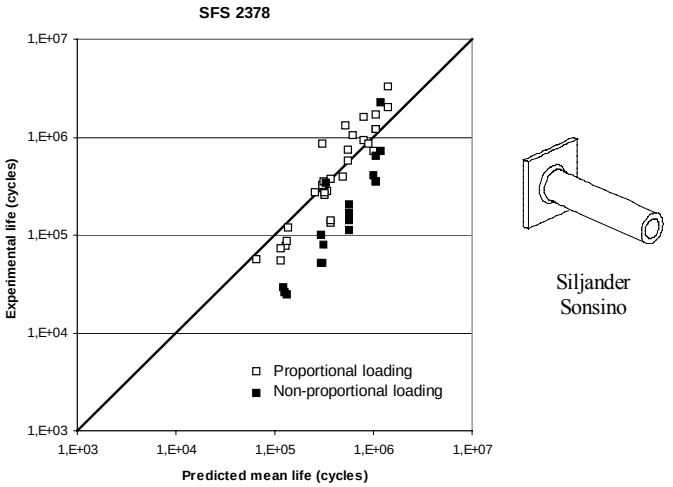

Figure 41. Re-evaluation of tube-to-plate welded joints under proportional and non-proportional loading using mean S-N curves and interaction equations from SFS 2378 (1992).

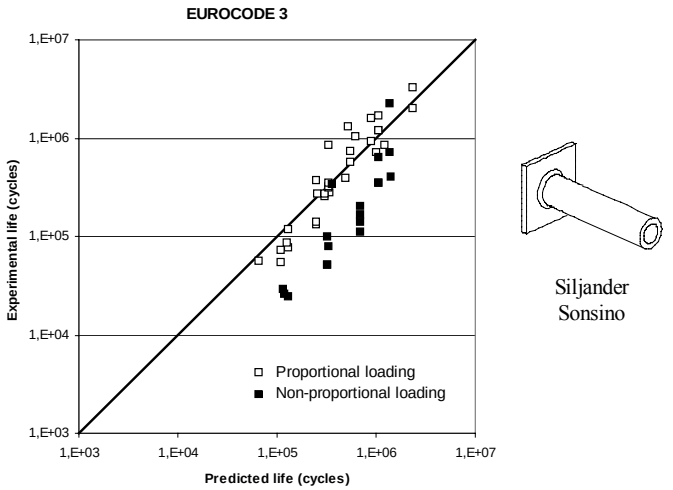

Figure 42. Re-evaluation of tube-to-plate welded joints under proportional and non-proportional loading using mean S-N curves and interaction equations from Eurocode 3 (1992).

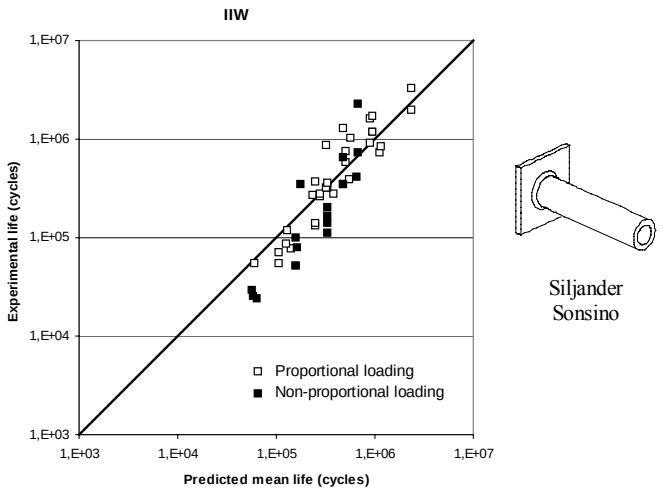

Figure 43. Re-evaluation of tube-to-plate welded joints under proportional and non-proportional loading using mean S-N curves and interaction equations from IIW recommendations.

5.3 Damage parameters

As seen from Figure 29, Figure 31, and Figure 33, the tube-tube test results tended to have the shortest fatigue life for a given stress parameter while the rectangular hollow section tests tended to have the longest fatigue lives. For the rectangular hollow section-to-plate welds, the hot spot stress distribution at the corner consisted of two components: membrane stress and shell bending stress. Membrane stress is the average stress through the plate thickness while shell-bending stress is one half of the difference between the stress values at the top and bottom surface. The hot spot stress was calculated by multiplying the nominal stress value with the stress concentration factor (SCF) obtained with FE calculations. The SCF does not consider stress gradients and does not differentiate between membrane and bending stress. During the total life of welded components with the same SCF, fatigue cracks grow faster in specimens with greater membrane stress than in specimens with greater shell bending stress. This may be one reason why the computed stress values for the rectangular hollow section specimen are overly conservative. Also, the region of high stress concentration is very small near the square hollow section corner and cracks quickly grow away

from this highly stressed region. The small region also means that there is a lesser chance of having a significant defect.

It is interesting to note that Razmjoo's test results were toward the upper end of the scatter band when analysed using the critical plane method, Figure 33, but toward the lower end of the scatter band when the maximum principal stress and maximum shear stress approaches were used, Figure 29 and Figure 31. These specimens were of higher yield strength steel and this indicates that the assumption of how residual stresses act on the critical plane may need to be modified for non-stress relieved joints. Razmjoo's test specimens were loaded with axial tension as compared to the other test series with bending loading. Under axial tension, a greater area of weld is subject to high stress as compared to bending. This means that welding flaws such as weld start/stop, porosity, slag inclusion, lack of fusion or incomplete weld root penetration are more likely to be in a highly stressed region during axial tension. Such flaws provide additional stress concentration that may lead to a reduction in fatigue life. Also the plate thickness of Razmjoo's test specimen were reduced from 7 mm to 3 mm at the ends of the tube. This may produce additional bending stresses at the weld toe due to eccentricity. Possible bending stresses were not considered in the current analysis.

The effect of proportional and non-proportional loading is seen in Figure 30, Figure 32 and Figure 34, which consider only a subset of the data. These figures show only the circular tube-to-plate specimens tested by Siljander et al. (1992) and Sonsino (1995, 1997). Results for proportional and non-proportional loading correlate better for the lower stress levels than at the higher stresses. When data was analysed using the maximum principal stress method, Figure 30, non-proportional loading was clearly more damaging than proportional loading. This confirms that the maximum principal stress range may not be used for nonproportional loading. The maximum shear stress method, Figure 32, accounted slightly better for the non-proportional loading, but did not unify the bending only and torsion only data into a single line. The critical plane approach, Figure 34, did the best job of unifying the four loading modes to a single stress vs. life-line. However, non-proportional loading still tended to be more damaging and further work on the method is needed.

Scatter in the test results was significant regardless of the analysis method used. In many cases the structural stress at the weld toe may be different from the hot spot stress assumed in the analysis. The tube-tube test results tended to have the shortest fatigue life for a given stress parameter. The apparent short fatigue life for these specimens may be partly explained by the low stress concentration factor, $K_s = 1$, assumed in the analysis. Butt welds such as the tube to tube joint may also have small offset or angular misalignments that can increase the hot spot stress. IIW recommendations (Hobbacher 1996) observes that misalignment stresses are automatically included if strain gage techniques are used to determine hot spot stresses but should also be taken into consideration when using numerical procedures. He also notes that butt welds may have greater or lesser fatigue strength as compared to fillet welds depending on the shape of the weld toe.

Because of this added uncertainty in evaluating the butt welds, Figure 44 shows only the 163 fillet weld specimens where failure occurred at the weld toe. As in Figure 33, the critical plane method is used assuming a damage slope of 3. The standard deviation in log(C) is reduced from $s = 0.47$ based on all data to $s = 0.41$ based on the fillet weld data. The computed design line increases from FAT 97 to FAT 114. The design fatigue strength curves for fillet welds were FAT 85 for maximum principal stress range and FAT 116 for maximum shear stress range. For comparison, hot spot stress vs. life data for about 100 axially loaded specimens have been reported by Partanen and Niemi (1996). The standard deviation in log(C) was 0.24, i.e., about 50–60% of what is observed here for multiaxial loaded welds.

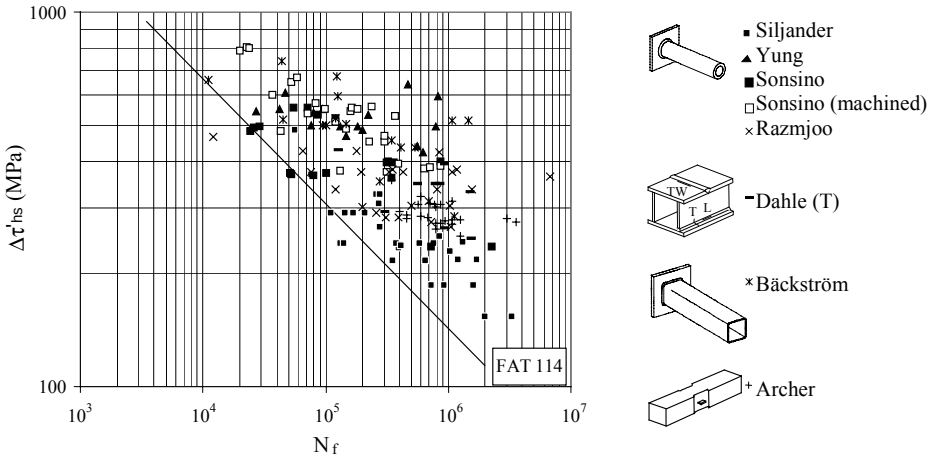

Figure 44. Fatigue test results for fillet welded joints under multiaxial loading using the hot spot critical plane approach.

Some of the scatter seen here is probably a result of differences in defining fatigue failure. The precise failure criterion was not reported in most of the studies reviewed but it was considered to be final break-through or collapse of the test component. Some studies additionally published the life to crack initiation, e.g., life to 1 mm crack depth. Crack initiation life could not be used since it was not available for most of the test pieces even though the critical plane model would be expected to better correlate initiation life than final fracture. Studies of non-welded fatigue specimens clearly show that crack growth mode changes as the fatigue process progresses (Socie 1993). Maximum shear stress and shear based critical plane models are more suitable for modelling the growth of short cracks or cracks subject to mode II/III loading while long cracks subject to mode I loading tend to grow along maximum principal stress planes. A single damage model is expected to be successful for complex loading only if it models the fatigue process that dominates fatigue life.

Further work is required particularly with respect to the effect of residual stresses. This could, in part, be done by using recently reported uniaxial data where weld geometry and residual stresses have been carefully measured (Lopez et al. 1999).

6. Conclusions

The majority of biaxial fatigue data for welded joints has focused primarily on proportional loading. A total of only 77 non-proportional data points for 7 specimen geometries have been reported. The current thesis examines 233 experimental results that produced weld toe failure from eight different studies. These have been analysed using six different methods. The methods are based on nominal and hot spot stresses using interaction equations, the maximum principal stress range, maximum shear stress range, and a critical plane model. Hot spot stresses were determined by multiplying nominal stress values published in the literature with a stress concentration factor. Some of the hot spot stress concentration factors were known from FE analysis while others were estimated or based on parametric formulae.

All interaction equations used with design fatigue classes tended to give conservative results but the scatter was greater than that observed for uniaxial loading cases and the degree of conservatism was specimen-type dependent. Of the three methods SFS 2378 provided the least degree of scatter when design fatigue classes were used. Of the three interaction equations considered with mean fatigue classes, the IIW most successfully correlated the predicted and experimental lives. However, the differences were not large. Interaction equations work best in cases where both the normal stress and the shear stress tend to produce crack in the same location and in the same direction. For tube-to-plate specimens the use of a damage summation of 0.5 for nonproportional loading in IIW was consistent with experimental observations. Other codes used a damage sum of unity.

Of the three damage parameters, the critical plane model was most successful in resolving the data to a single S-N line. However, observed scatter was 70–100% larger than that observed in uniaxial loaded specimens analysed by using the hot spot approach. Scatter can be attributed to differences in specimen geometries, test methods, plate thicknesses and the definition of failure. The maximum principal stress range and the maximum shear stress range could not explain the increased damage normally observed during nonproportional loading as compared to proportional loading. Even the critical plane model needs improvement

in explaining the increased damage. The method of accounting for residual stresses and the definition of possible damage planes also requires further work.

The design hot spot S-N curves were FAT 84 for maximum principal stress range, FAT 109 for maximum shear stress range and FAT 97 for the modified critical plane model, when all toe failures were analysed with a slope of 3. By excluding butt welds and including only fillet welds that failed at the weld toe, the design curves were increased to FAT 85 for maximum principal stress range, FAT 116 for maximum shear stress range and FAT 114 for the modified critical plane model with a slope of 3.

The present thesis is limited to nominal and hot spot stresses, which do not describe the real damaging components of stress tensor at the weld toe. Consequently, the application of a local stress approach in combination with an appropriate hypothesis depending on materials ductility is left for future work. Finally, it should be pointed out that the definition of biaxial and multiaxial loading should be clarified in the design codes, because the design codes do not give methods for designers to distinguish proportional loading from the non-proportional loading in complex operational load histories.

References

Almar-Naess, A. 1985. Fatigue handbook. Offshore steel structures. Norge: Tapir. 520 p. ISBN 82-519-0662-8

Archer, R. 1987. Fatigue of a welded steel attachment under combined direct stress and shear stress. In: International conference on fatigue of welded constructions. Brighton, UK: The Welding Institute. Paper No. 50. Pp. P50.1–P50.10.

ASME 1989. ASME boiler and pressure vessel code. Section III, Rule for construction of nuclear power plant components. New York, USA: The American society of mechanical engineers. (Division 1 – Subsection NB, Class 1 components.)

Bannantine, J.A., Comer J.J., Handrock J.L. 1990. Fundamentals of metal fatigue analysis. New Jersey: Prentice–Hall. 273 p. ISBN 0-13-340191-X.

Becker, A.A. 1992. The boundary element method in engineering. A complete course. England: McGraw–Hill Book Company Europe. 337 p. ISBN 0-07-707415-7

Broek, D. 1988. The practical use of the fracture mechanics. The Netherlands: Kluwer Academic Publishers. 522 p.

Brown, M.W., Miller, K.J. 1973. A theory for fatigue failure under multiaxial stress-strain conditions. Proceedings of the Institute of Mechanical Engineers, Vol. 187 (65/73), pp. 745–756.

Bäckström, M., Kähönen, A., Liukkonen, S., Rönnskog, R., Bonde, M. 1997b. Structural integrity assessment of a truck trailer. In: Blom, A.F. (ed.). Welded High-Strength Steel Structures. Proceedings of the First North European Engineering and Science Conference (NESCO I), Sweden, Stockholm 8–9 October. London: EMAS Publishing. Pp. 527–541. ISBN 0 947817 95 6

Bäckström, M., Marquis, G. 2001a. Evaluation of interaction equations for multiaxial loaded welded joints. In: Proc. 6th Intl. Conf. Biaxial/Multiaxial Fat. and Fract. de Freitas, M.M. (ed.). IST: Lisbon. Pp. 65–72.

Bäckström, M., Marquis, G. 2001b. A review of multiaxial fatigue of weldments: experimental results, design code and critical plane approaches. Fatigue and Fracture of Engineering Materials & Structures. Vol. 24, pp. 279–291.

Bäckström, M., Mikkola, T.P.J., Marquis, G., Ortmans, O. 2000. Testing and analysis of window details for passenger ships. In: Bache, M.R., Blackmore, P.A., Draper, J., Edwards, J.H., Roberts, P., Yates, J.R. (ed.). Fatigue 2000, Fatigue & durability assessment of materials, components and structures. U.K: EMAS. Pp. 335–344. ISBN 1 901537 16 1

Bäckström, M., Siljander, A., Kuitunen, R., Ilvonen, R. 1997a. Multiaxial Fatigue Experiments of Square Hollow Section Tube-to-Plate Welded Joints. In: Blom, A.F. (ed.). Welded High-Strength Steel Structures. Proceedings of the First North European Engineering and Science Conference (NESCO I), Sweden, Stockholm 8–9 October. London: EMAS Publishing. Pp. 163–177. ISBN 0 947817 95 6

Dahle, T., Olsson, K.-E., Jonsson, B. 1997. High Strength Welded Box Beams Subjected to Torsion and Bending – Test Results and Proposed Design Criteria for Torsion/Bending Interaction. In: Blom, A.F. (ed.). Welded High-Strength Steel Structures. Proceedings of the First North European Engineering and Science Conference (NESCO I), Sweden, Stockholm 8–9 October. London: EMAS Publishing. Pp. 143–161. ISBN 0 947817 95 6

Dutta, D., Sedlacek, G., Stranghöner, N. 1996. Design Guide for Hollow Section Structures Under Fatigue Loading, Working Draft. Aachen: RWTH. 113 p. (CIDECT Research Project 7M.)

Eurocode 3, 1992. Design of steel structures – Part 1-1: General rules and rules for buildings. (ENV 1993-1-1.)

Fatemi, A., Yang, L. 1998. Cumulative fatigue damage and life prediction theories: a survey of the state of the art for homogeneous materials. International journal of fatigue. U.K: Elsevier Science Ltd. Vol. 20, No. 1, pp. 9–34.

Findley, W.N. 1959. A theory for the effect of mean stress on fatigue of metals under combined torsion and axial load or bending. Journal of Engineering for Industry, pp. 301–306.

Fuchs, H.O., Stephens, R.I. 1980. Metal Fatigue in Engineering. USA, New York: John Wiley & Sons. 318 p. ISBN 0-471-05264-7

Gurney, T.R. 1979. Fatigue of welded structures. 2nd edition. UK: Gambridge University Press. 456 p. ISBN 0 521 22558 2

Hobbacher, A. 1996. Recommendations for fatigue design of welded joints and components. ISO standard proposal. 127 p. (IIW document XIII-1539-96 / XV-845-96.)

Iida, K., Uemura, T. 1996. Stress concentration factor formulae widely used in Japan. Fatigue & Fracture of Engineering Materials & Structures, Vol. 19, No. 6, pp. 779–786.

Lehtonen, M. 1997. On the evaluation of the hot spot stresses using FEM. In: Blom, A.F. (ed.). Welded High-Strength Steel Structures. Proceedings of the First North European Engineering and Science Conference (NESCO I), Sweden, Stockholm 8–9 October. London: EMAS Publishing. Pp. 225–239. ISBN 0 947817 95 6

Lopez Martinez, L., Lin Peng, R., Blom, A.F., Wang, D.Q. 1999. Welding and TIG-Dressing Induced Residual Stresses – Relaxation and Influence on Fatigue Strength of Spectrum Loaded Weldments. In: Marquis, G., Solin, J. (ed.). Fatigue Design and Reliability. U.K: ESIS. Pp. 117–133. (ESIS Publication 23.) ISBN 008 043329 4

Maddox, S.J. 1991. Fatigue strength of welded structures. 2nd ed. Cambridge, England: Abington Publishing. 198 p. ISBN 1 85573 013 8

Marquis, G., Bäckström, M., Siljander, A. 1997. Multiaxial fatigue damage parameters for welded joints: Design code and critical plane approaches. In: Blom, A.F. (ed.). Welded High-Strength Steel Structures. Proceedings of the First

North European Engineering and Science Conference (NESCO I), Sweden, Stockholm 8–9 October. London: EMAS Publishing. Pp. 127–141.

Marquis, G.B. 1995. High cycle spectrum fatigue of welded components. Thesis. Espoo: Technical Research Centre of Finland. 83 p. + app. 100 p. (VTT Publications 240).

Miller, K.J. 2000. Blind alleys on the route to fatigue-failure solutions: a historical perspective. In: Bache, M.R., Blackmore, P.A., Draper, J., Edwards, J.H., Roberts, P., Yates, J.R. (ed.). Fatigue 2000, Fatigue & durability assessment of materials, components and structures. U.K: EMAS. Pp. 3–14.

Niemi, E. 1995. Stress Determination for Fatigue Analysis of Welded Components. UK, Abington: Abington Publishing. 69 p. (IIW Doc IIS/IIW-1221-93.)

Niemi, E. 1996. Analysis of variable amplitude fatigue using equivalent constant amplitude stress range. In: Kähönen, A., Moring, E. (ed.). Väsymismitoitus 1996. Espoo: Technical Research Centre of Finland. Pp. 7–19. (VTT Symposium 166.) ISBN 951-38-4557-5

Niemi, E., Kilkki, J., Poutiainen, I., Lihavainen, V.-M. 1998. Väsymättömän hitsausliitoksen suunnittelu [Fatigue free design of welded joints]. Lappeenranta, Finland: LTKK monistuspalvelu. 149 p. (In Finnish.)

Nykänen, T. 1993. Mk-Factor Equations and Crack Growth Simulations for Fatigue of Fillet-Welded T-Joints. Lappeenranta: Lappeenranta University of Technology. 198 p. (Research papers 31.) ISBN 951-763-793-4

Ohta, A., Matsuoka, K., Suzuki, N., Maeda, Y. 1994. Fatigue strength of non-load-carrying cruciform welded joints by a test maintaining maximum stress at yield strength. Engineering fracture mechanics, Vol. 49, No. 4, pp. 639–645.

Paris, P., Erdogan, F. 1963. A critical analysis of crack propagation laws. Journal of Basic Engineering. Transactions of the ASME, Series D, Vol. 85, pp. 528–534.

Partanen,T., Niemi, E., 1996. Hot spot stress approach to fatigue strength analysis of welded components: fatigue test data for steel plate thicknesses up to 10 mm. Fatigue & Fracture of Engineering Materials & Structures, Vol. 19, No. 6, pp. 709–722.

PD 6493. 1991. Guidance on methods for assessing the acceptability of flaws in fusion welded structures. London: British Standards Institution. 120 p. (Published document 6493:1991.) ISBN 0 580 19634 8

Pook, L.P. 1994. Mixed mode fatigue crack propagation. Carpinteri, A. (ed.). Handbook of fatigue crack propagation in metallic structures. Netherlands: Elsevier Science B.V.Vol. 2. Pp. 1027–1071. ISBN 0 444 818453

Pook, L.P., Grawford, D.G. 1991. The fatigue crack direction and threshold behaviour of a medium strength structural steel under mixed mode I and II loading. In: Kussmaul, K.F., McDiarmid, Socie, D.F. (ed.). Fatigue under biaxial and multiaxial loading. U.K: ESIS. Pp. 199–211. (ESIS Publication 10.) ISBN 0 85298 770 6

Razmjoo, G.R. 1996. Fatigue of load-carrying filled welded joints under multiaxial loading. Abington Hall, Abington Cambridge, United Kingdom: TWI. Pp. 10. (TWI Ref. 7309.02/96/909)

Ritchie, R.O., McClintock, F.A., Tschegg, E.K., Nayeb-Hashemi, H. 1982. Mode III fatigue crack growth under combined torsional and axial loading. In: Miller, K.J., Brown, M.W. (ed.). Multiaxial fatigue. USA: ASTM. Pp. 203–227. (ASTM STP 853.) ISBN 0 8031 0444 8

SAE AE-10. 1988. Fatigue Design handbook. 2nd ed. USA: Society of Automotive Engineers. 369 p. ISBN 0-89883-011-7

SAE AE-14. 1989. Multiaxial fatigue: Analysis and Experiments. USA: Society of Automotive Engineers. 162 p. ISBN 0-89883-780-4

SFS 2378. 1992. Welding. Load capacity of welded joints in fatigue loaded steel structures. Helsinki: Finnish Standards Association SFS. 51 p.

Siljander, A., Kurath, P., Lawrence, F.V. Jr. 1992. Nonproportional fatigue of welded structures. In: Mitchell, M.R., Landgraf, R.W. (ed.). Advances in fatigue lifetime predictive techniques. USA: ASTM. Pp. 319–338. (ASTM STP 1122.) ISBN 0 8031 1423 0

Siljander, A., Kähönen, A., Lehtonen, M., Juntunen, J., Mäntysaari, P. 1997a. Development of a straddle carrier wheel support. In: Blom, A.F. (ed.). Welded High-Strength Steel Structures. Proceedings of the First North European Engineering and Science Conference (NESCO I), Sweden, Stockholm 8–9 October. London: EMAS Publishing. Pp. 471–485. ISBN 0 947817 95 6

Siljander, A., Kähönen, A., Lehtonen, M., Nurminen, S., Lundahl, K. 1997b. Durability assessments of armoured personnel carrier axle housing. In: Blom, A.F. (ed.). Welded High-Strength Steel Structures. Proceedings of the First North European Engineering and Science Conference (NESCO I), Sweden, Stockholm 8–9 October. London: EMAS Publishing. Pp. 505–518. ISBN 0 947817 95 6

Socie, D. 1993. Critical plane approaches for multiaxial fatigue damage assessment. In: McDowell, D.L., Ellis, R. (ed.). Advances in multiaxial fatigue. USA: ASTM. Pp. 7–36. (ASTM STP 1191.) ISBN 0 8031 1862 7

Socie, D.F., Furman, S. 1996. Fatigue damage simulation models for multiaxial loading. In: Lűtjering, G., Nowack, H. (ed.). Fatigue '96, Proceedings of sixth international fatigue congress, Volume II. U.K: Pergamon. Pp. 967–976. ISBN 0 08 042268 3

Socie, D.F., Marquis, G.B. 2000. Multiaxial fatigue. USA: SAE International. ISBN 0 7680 0453 5

Sonsino, C.M. 1995. Multiaxial fatigue of welded joints under in-phase and out-of-phase local strains and stresses. International journal of fatigue, Vol. 17, No. 1, pp. 55–70.

Sonsino, C.M. 1997. Schwingfestigkeit von geschweißten komponenten unter komplexen elasto-plastischen, mehrachsigen verformungen. Darmstadt: Fraunhofer Institut Betriebsfestigkeit and Luxembourg: Commission of European Communities. (LBF-Nr. 6078 and EUR-report No. 16024)

Sonsino, C. M., and Maddox, S. J. 2001. Multiaxial fatigue of welded structures. Problems and present solutions. In: Proc. 6th Intl. Conf. Biaxial/Multiaxial Fat. and Fract. de Freitas, M.M. (ed.). IST: Lisbon. Pp. 3–15.

Timoshenko, S.P., Goodier, J.N. 1982. Theory of Elasticity. 3nd ed. Singapore: McGraw–Hill Book Co. 567 p. ISBN 0-07-Y85805-5

Wardenier, J., Dutta, D., Yeomans, N., Packer, J.A., Bucak, Ö. 1995. Design Guide for Structural Hollow Sections in Mechanical Applications. Germany: Verlag TUV Rheinland. 157 p. (CIDECT Construction with Hollow Steel Sections.) ISBN 3-8249-0302-4

Wingerde, A.M. 1992. The Fatigue Behaviour of T- and X-Joints Made of Square Hollow Sections. Thesis. 182 p.

Yu, H.C., Tanaka, K., Akiniwa, Y. 1998. Estimation of torsional fatigue strength of medium carbon steel bars with a circumferential crack by the cyclic resistance-curve method. Fatigue & Fracture of Engineering Materials & Structures. Vol. 21, pp. 1067–1076.

Yung, J.-Y., Lawrence, F.V. Jr. 1986. Predicting the fatigue life of welds under combined bending and torsion. Urbana-Champaign: University of Illinois. 27 p. (UILU-ENG 86-3602, Report No. 125)

Zhang, Z. 1994. A Practical Micro-Mechanical Model-Based Local Approach Methodology for the Analysis of Ductile Fracture of Welded T-Joints. Lappeenranta: Lappeenranta University of Technology. 151 p. (Research Papers 34.) ISBN 951-763-837-X

Zheng, X.-L. 1994. Mechanical model for fatigue crack propagation in metals. In: Carpinteri, A. (ed.). Handbook of Fatigue Crack Propagation in Metallic Structures. Netherlands: Elsevier Science B.V. Vol. 1, pp. 363–395. ISBN 0 444 816453

Appendix A: Example calculation for critical plane approach

Assume that the tube-to-plate test specimen shown in Figure 11 is subjected to proportional constant amplitude bending and torsion loading. The nominal normal stress range at the weld toe is $\Delta\sigma_{nom}$ = 100 MPa with a nominal normal stress ratio of R_σ = 0 and the nominal shear stress range at the weld toe is $\Delta\tau_{nom}$ = 60 MPa with a nominal shear stress ratio of R_τ = -1. This loading is illustrated in Figure A1a. Structural stress concentration factors are assumed to be $K_{s,\sigma}$ = 3 for normal stress and $K_{s,\sigma}$ = 1.3 for shear stress. The assumed stress history at the hot spot is obtained simply by multiplying the nominal stress by the structural stress concentration factors with the result shown in Figure A1b. The tube-to-plate specimen is tested as-welded and the yield strength of the tube is σ_y = 355 MPa and the normal stress sensitivity factor is assumed to be k = 0.3.

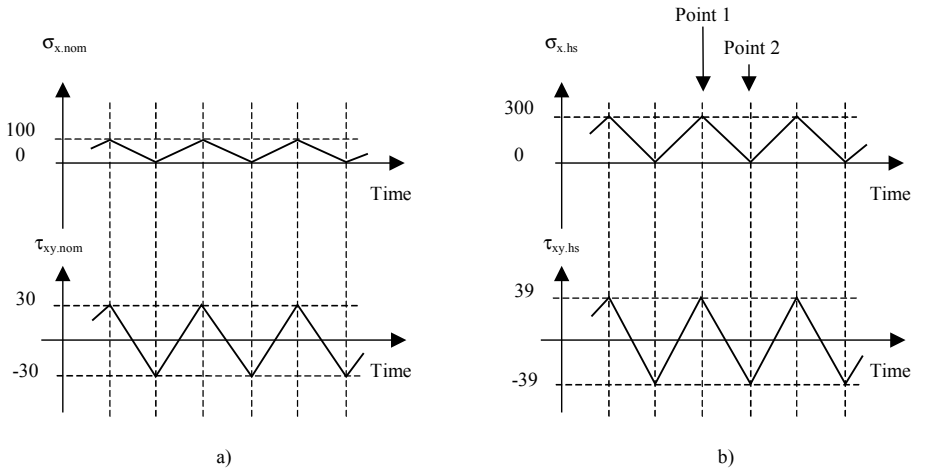

Figure A1. a) The nominal and b) hot spot normal and shear time histories at the weld toe for tube-to-plate test specimen.

Hot spot stresses at points in time and on different planes are easily computed using the equilibrium Eq. (30). Because the loading in this example is proportional and constant amplitude, it is sufficient to calculate stresses for two points in the time history. These are indicated as Point 1 and Point 2 in Figure A1b. With reference to Figure 11, potential critical planes are assumed to be $\theta = 0°$ with angle ϕ varying from -45° to 45°. Damage varies slowly from plane to plane so in this case damage was computed for planes at 15° intervals. From Eq. (30) two shear stresses on the plane are calculated, $\tau_{x'y'}$ and $\tau_{x'z'}$. These two vector quantities combine to produce a resultant shear stress on the plane. Both the direction and magnitude of this resultant shear change with time. An angle ψ is introduced to indicate the direction of shear (see Figure A2). The magnitude of shear stress corresponding to $\psi = 0°$ to 90° is then computed at both points in time.

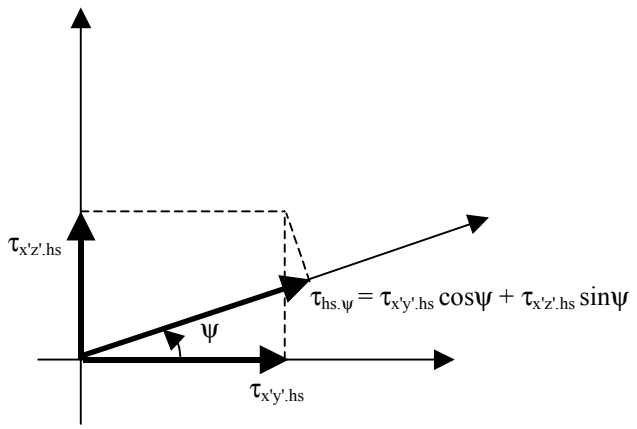

Figure A2. Co-ordinate transformation of shear stresses on a potential critical plane.

For non-stress relieved structures, the normal stress on a plane is derived for the maximum of the σ_y or the maximum applied hot spot stress. In this example the σ_y = 355 MPa while the maximum hot spot stress during a cycle is only 300 MPa. Table AI shows the hot spot shear stress on different planes (ϕ) and in different directions (ψ) at the two points in time. Table AII presents the hot spot shear stress ranges determined from Table AI, the maximum hot spot normal stress, see Eq. (30), and effective hot spot shear stress range in Eq. (29) resolved on to various planes (ϕ). For k = 0.3, the largest value of the damage parameter,

$\Delta\tau'_{hs}$ = 306 MPa, is found to occur on the plane ϕ = -30° with the shear direction ψ = 60°. Same maximum damage $\Delta\tau'_{hs}$ can be found on other planes e.g. varying angle ψ from -90° to 0°. It can be noted that on the ϕ = -30° plane, the maximum shear stress at Point 1 is in the direction ψ = 75° and the minimum shear stress at Point 2 is in the direction ψ = 0°. However, the maximum range during the entire load cycle is in the direction ψ = 60°. It can also be noted that the maximum value of $\Delta\tau'_{hs}$ does not occur on the plane of maximum shear stress nor on the plane of maximum normal stress.

Table AI. Resultant hot spot shear stresses ($\tau_{hs.\psi}$) on different planes (ϕ) and directions (ψ).

Time history	ψ \ ϕ	-45°	-30°	-15°	0°	15°	30°	45°
Point 1	0	27.6	33.8	37.7	39.0	37.7	33.8	27.6
	15	65.5	66.2	55.8	37.7	17.0	-1.0	-12.2
	30	98.9	94.2	70.1	33.8	-4.9	-35.7	-51.1
	45	125.6	115.7	79.7	27.6	-26.4	-68.0	-86.6
	60	143.7	129.4	83.8	19.5	-46.1	-95.6	-116.1
	75	152.0	134.2	82.2	10.1	-62.7	-116.7	-137.8
	90	150.0	129.9	75.0	0.0	-75.0	-129.9	-150.0
Point 2	0	-27.6	-33.8	-37.7	-39.0	-37.7	-33.8	-27.6
	15	-26.6	-32.6	-36.4	-37.7	-36.4	-32.6	-26.6
	30	-23.9	-29.3	-32.6	-33.8	-32.6	-29.3	-23.9
	45	-19.5	-23.9	-26.6	-27.6	-26.6	-23.9	-19.5
	60	-13.8	-16.9	-18.8	-19.5	-18.8	-16.9	-13.8
	75	-7.1	-8.7	-9.8	-10.1	-9.8	-8.7	-7.1
	90	0.0	0.0	0.0	0.0	0.0	0.0	0.0

Table AII. Alternating hot spot shear stress, maximum hot spot normal stress and effective hot spot shear stress range on different planes and directions during the load cycle.

$\Delta\tau_{hs.\psi} = \tau_{hs.\psi}^{\text{Point 1}} - \tau_{hs.\psi}^{\text{Point 2}}$							
$\psi \setminus \phi$	-45°	**-30°**	-15°	0°	15°	30°	45°
0	55.2	67.5	75.3	78.0	75.3	67.5	55.2
15	92.1	98.9	92.2	75.3	53.4	31.6	14.5
30	122.8	123.5	102.7	67.5	27.7	6.5	27.2
45	145.1	139.6	106.3	55.2	0.2	44.1	67.1
60	157.5	**146.3**	102.6	39.0	27.3	78.7	102.3
75	159.2	143.0	91.9	20.2	52.9	108.0	130.6
90	150.0	129.9	75.0	0.0	75.0	129.9	150.0
$\sigma_{n,hs}^{max}$	177.5	**266.3**	331.2	355.0	331.2	266.3	177.5
$\Delta\tau'_{hs}$	265.7	**306.0**	305.0	291.0	274.0	289.7	256.5

Design curve for fillet welds based on the critical plane model and hot spot stresses is FAT 114 with a slope of 3, see Figure 44. Thus, the material constant for critical plane hot spot strength curve in Eq. (29) is

$$\tau_f^* = \left(114^3 \cdot 2 \cdot 10^6\right)^{\frac{1}{3}} = 14363 \tag{A1}$$

with a slope of b = -1/3. The fatigue life for the test specimen can be calculated from Eq. (29) and Table AII

$$N_f = \left(\frac{\Delta\tau'_{hs}}{\tau_f^*}\right)^{\frac{1}{b}} = \left(\frac{306}{14363}\right)^{-3} = \underline{103000\ cycles} \tag{A2}$$

This example deals with proportional constant amplitude bending and torsion loading where only the turning points in the time history are analysed (Table AI). Instead, for non-proportional loading all data points in the time history should be checked.

Appendix B: Example of application effective equivalent stress hypothesis

Maximum Distortion Energy Hypothesis (von Mises) and Effective Equivalent Stress Hypothesis (EESH)
MBA 29.10.-97

(Sub)scripts:		
	a	amplitude
	b, t	bending, torsion
	d	design
	m	mean
	x, y, z	coordinates

Initial values

Fatigue design strength f_d

$f_{dx} := 383$ $f_{dy} := 0$ $f_{dxy} := 275$

The slopes m_1 ($N \le N_d$) and m_2 ($N > N_d$) of the bilinear S-N curve for welded joints

$N_d := 2 \cdot 10^6$ $m_1 := 5$

Size effect factor which is determined by comparing the S-N-curve for pure axial or bending stress with that for pure torsion on the basis of local supportable stresses

$f_0 := \frac{f_{dx}}{f_{dxy}}$ $f_0 = 1.393$

Frequence f, angular velocity ω and phase displacement δ

$f := 1$ $\omega_x := 2 \cdot \pi \cdot f$

$\omega_y := \omega_x$ $\delta_y := 0$

$\omega_{xy} := \omega_x$ $\delta_{xy} := 90 \cdot deg$

Bending or normal stresses σ (local), shear stresses τ (local), the stress concentration factors ($K_{tb} = \sigma_x / \sigma_n$ and $K_t = \tau_{xy} / \tau_n$) and the ratio of stress concentration factors G

$\sigma_{ax} := 637$ $\sigma_{mx} := 0$ $K_{tb} := 3.93$

$\sigma_{ay} := 178$ $\sigma_{my} := 0$

$\tau_{axy} := 179$ $\tau_{mxy} := 0$ $K_{tt} := 1.85$

$G := \frac{1 + K_{tb}}{1 + K_{tt}}$ $G = 1.73$

The biaxial stress state at the weld toe (notch ground surface) generated by sinusoidal combined bending and torsion can be written as

$$\sigma_x(t) := \sigma m_x + \sigma a_x \cdot \sin(\omega_x \cdot t)$$

$$\sigma_y(t) := \sigma m_y + \sigma a_y \cdot \sin(\omega_y \cdot t - \delta_y)$$

$$\tau_{xy}(t, \delta_{xy}) := \tau m_{xy} + \tau a_{xy} \cdot \sin(\omega_{xy} \cdot t - \delta_{xy})$$

The EESH assumes that the failure of ductile materials under multiaxial stress state is initiated by shear stresses τ_ψ. Shear stress of the biaxial stress-state on different interference planes is

$$\tau_\psi(\psi, t, \delta_{xy}) := \frac{\sigma_x(t) - \sigma_y(t)}{2} \cdot \sin(2 \cdot \psi) - \tau_{xy}(t, \delta_{xy}) \cdot \cos(2 \cdot \psi)$$

For non-proportional stress states, the interaction of shear stresses in various interference planes ψ is taken into account by generating an effective shear stress

$$\tau a_{with}(\tau a_\psi) := \frac{\sum_{k=0}^{17} \tau a_{\psi_k}}{18}$$

$\tau a_\psi(\delta_{xy}) :=$ for $k \in 0..17$

  $\tau_{max} \leftarrow -\infty$

  $\tau_{min} \leftarrow \infty$

  for $i \in 0..36$

    $\tau \leftarrow \tau_\psi\left(\frac{\pi}{18} \cdot k, \frac{i}{36}, \delta_{xy}\right)$

    $\tau_{max} \leftarrow \tau$ if $\tau \geq \tau_{max}$

    $\tau_{min} \leftarrow \tau$ if $\tau < \tau_{min}$

  $\tau a_{\psi_k} \leftarrow \frac{\tau_{max} - \tau_{min}}{2}$

τa_ψ

$\tau a_\psi(0) =$ (179, 90, 10, 109, 195, 257, 288, 285, 247, 179, 90, 10, 109, 195, 257, 288, 285, 247)

$\tau a_\psi(\delta_{xy}) =$ (179, 185, 201, 217, 228, 228, 217, 201, 185, 179, 185, 201, 217, 228, 228, 217, 201, 185)

$\max(\tau a_\psi(0)) = 288$ $\quad \max(\tau a_\psi(\delta_{xy})) = 228$

$\tau a_{with}(\tau a_\psi(0)) = 184$ $\quad \tau a_{with}(\tau a_\psi(\delta_{xy})) = 205$

The nominal design curve must be transformed into a local one in multiaxial stress state because the incorrect use of combined nominal stress components results in an underestimation of fatigue life. Which means that the effect of the shear stress in relation to the normal stress is overestimated. The local stress based modification of von Mises is

$$\sigma a_{eq\_vonMises} := \sqrt{\sigma a_x^{\,2} + \sigma a_y^{\,2} - \sigma a_x \cdot \sigma a_y + 3 \cdot \tau a_{xy}^{\,2}}$$

$\sigma a_{eq\_vonMises} = 648$

$$N := \frac{N_d \cdot f_{dx}^{\,m_1}}{\sigma a_{eq\_vonMises}^{\,m_1}}$$

$N = 144016$

However, the physically correct use of local maximum stresses does not always result in a correct equivalent stress if the von Mises hypothesis is applied. This hypothesis is only valid for proportional multiaxial loading with not changing principal stress directions. The hypothesis of effective equivalent stress (EESH) was developed to overcome the limitations of the von Mises criterion. The first modification is the size effect factor f_G which reflects the influence of the maximum stressed material volume on the supportable local stress. For the proportional multiaxial loading EESH is

$$\sigma a_{eq\_\delta xy0} := \sqrt{\sigma a_x^{\,2} + \sigma a_y^{\,2} - \sigma a_x \sigma a_y + f_G^{\,2} \cdot 3 \cdot \tau a_{xy}^{\,2}} \qquad \sigma a_{eq\_\delta xy0} = 715$$

$$N := \frac{N_d \cdot f_{dx}^{\,m_1}}{\sigma a_{eq\_\delta xy0}^{\,m_1}} \qquad N = 88512$$

The effective shear stress is used to determining the EESH for the non-proportional multiaxial loading

$$\sigma a_{eq\_\delta xy} := \sigma a_{eq\_\delta xy0} \cdot \frac{\tau a_{arith}\left(\tau a_\psi\left(\delta_{xy}\right)\right)}{\tau a_{arith}\left(\tau a_\psi(0)\right)} \cdot \sqrt{G^{\,1-\left(\frac{2}{\pi}\cdot\delta_{xy}-1\right)^2}} \qquad \sigma a_{eq\_\delta xy} = 1043$$

$$N := \frac{N_d \cdot f_{dx}^{\,m_1}}{\sigma a_{eq\_\delta xy}^{\,m_1}} \qquad N = 13374$$

The root in the EESH equation considers the influence of the material volume affected by the rotating principal stress and principal strain axes on the magnitude of the effective equivalent strain in the case of a phase displacement according to a model developed for semiductile materials.

References

Sonsino, C.M. 1997. Schwingfestigkeit von geschweißten komponenten unter komplexen elasto-plastischen, mehrachsigen verformungen. Darmstadt: Fraunhofer Institut Betriebsfestigkeit and Luxembourg: Commission of European Communities. (LBF-Nr. 6078 and EUR-report No. 16024)

Sonsino, C.M. 1997. Multiaxial and Random Loading of Welded Structures. In: Maddox, S.J., Prager, M. (ed.) International Conference on Performance of Dynamically Loaded Welded Structures. IIW 50th Annual Assembly Conference Meeting Proceedings, San Francisco 14 -15 July. USA: Welding Research Council. p. 317-331. ISBN 0-9656164-9-5

Sonsino, C.M. 1997. Overview of the State of the Art on Multiaxial Fatigue of Welds. In: Macha, E., Mroz, Z. (ed.) Proceedings of the 5th International Conference on Biaxial/Multiaxial Fatigue & Fracture, Cracow 8 -12 September. Poland: Wydawnictwo Instytut Slaski Sp. z o.o. p. 395-419. ISBN 83-86706-40-9

Sonsino, C. M., and Maddox, S. J. 2001. Multiaxial fatigue of welded structures. Problems and present solutions. In: Proc. 6th Intl. Conf. Biaxial/Multiaxial Fat. and Fract., pp. 3-15, M. M. de Freitas (Ed.). IST: Lisbon.

Appendix C: Rectangular tube to plate test specimen

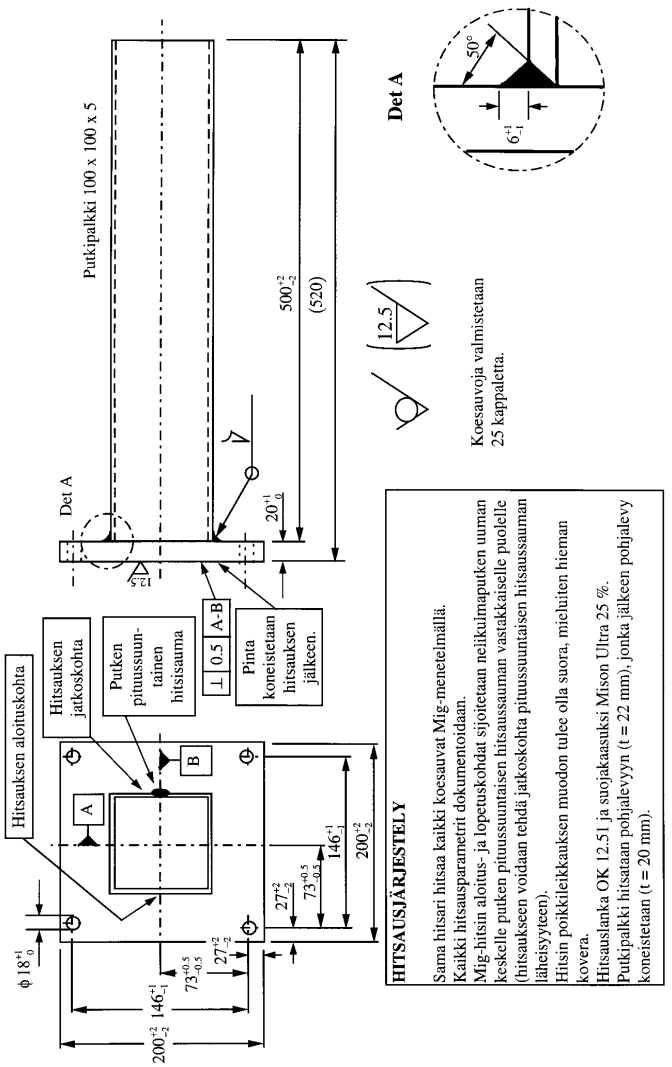

Published by

Series title, number and report code of publication

VTT Publications 502
VTT–PUBS–502

Author(s)
Bäckström, Mika

Title

Multiaxial fatigue life assessment of welds based on nominal and hot spot stresses

Abstract

A little attention has been focused on multiaxial fatigue of welded joints, even though numerous industrial applications require the consideration of multiaxial effects. Therefore, the goal in present thesis was to find methods for fatigue assessment of welded joints in multiaxial loading cases. A survey of biaxial (bending or tension and torsion) constant amplitude fatigue test results of welded connections was also carried out. Re-analysis of these 233 experimental results from eight different studies was performed based on nominal and hot spot stresses. Three potential interaction equations and three damage parameters were used in the re-analysis.

The interaction equations were obtained from SFS 2378, Eurocode 3 and IIW recommendations. Of the three interaction equations SFS 2378 provided the least degree of scatter when design fatigue classes were used and with mean fatigue classes the IIW most successfully correlated the predicted and experimental lives.

Principal stress range, maximum shear stress range, and a modified critical plane model for welds were used as the damage parameters. The design hot spot S-N curves were FAT 84 for maximum principal stress range, FAT 109 for maximum shear stress range and FAT 97 for the modified critical plane model, when all toe failures were analysed with a slope of 3. However, observed scatter was 70–100% larger than that observed in uniaxial loaded specimens analysed using the hot spot approach.

Keywords

fatigue life, assessments, nominal stresses, hot spot stresses, biaxial fatigue, multiaxial fatigue, welded joints, theses

Activity unit

VTT Industrial Systems, Otakaari 7 B, P.O.Box 1705, FIN–02044 VTT, Finland

ISBN			Project number
951–38–6233–X (soft back ed.) 951–38–6234–8 (URL:http://www.vtt.fi/inf/pdf/)			
Date	Language	Pages	Price
July 2003		97 p. + app. 9 p.	C
Name of project		Commissioned by	
Series title and ISSN		Sold by	
VTT Publications 1235–0621 (soft back ed.) 1455–0849 (URL: http://www.vtt.fi/inf/pdf/)		VTT Information Service P.O.Box 2000, FIN–02044 VTT, Finland Phone internat. +358 9 456 4404 Fax +358 9 456 4374	

Service loading of welded components is in numerous industrial application multiaxial which should be considered in the design stage of the welded structures. The publication addresses the question of which kind of methods should be used for fatigue assessment of welded components under multiaxial loading conditions. An experimental program including fatigue tests of rectangular welded tube-to-plate components and window corners from a passenger ferry have been performed. A critical plane fatigue assessment criterion based on the Findley model is modified to be more suitable for welded structures. A literature survey of previous multiaxial fatigue test results on welded joints has been conducted as well as a comparison and an evaluation of different standard methods.

Tätä julkaisua myy
VTT TIETOPALVELU
PL 2000
02044 VTT
Puh. (09) 456 4404
Faksi (09) 456 4374

Denna publikation säljs av
VTT INFORMATIONSTJÄNST
PB 2000
02044 VTT
Tel. (09) 456 4404
Fax (09) 456 4374

This publication is available from
VTT INFORMATION SERVICE
P.O.Box 2000
FIN–02044 VTT, Finland
Phone internat. +358 9 456 4404
Fax +358 9 456 4374

ISBN 951–38–6233–X (soft back ed.)
ISSN 1235–0621 (soft back ed.)

ISBN 951–38–6234–8 (URL: http://www.vtt.fi/inf/pdf/)
ISSN 1455–0849 (URL: http://www.vtt.fi/inf/pdf/)

VTT PUBLICATIONS 502 Multiaxial fatigue life assessment of welds based on nominal and hot spot stresses
Mika Bäckström